
Article:
Watson, CS, Quincey, DJ, Carrivick, JL et al. (2017) Ice cliff dynamics in the Everest region of the Central Himalaya. Geomorphology, 278. pp. 238-251. ISSN: 0169-555X

https://doi.org/10.1016/j.geomorph.2016.11.017

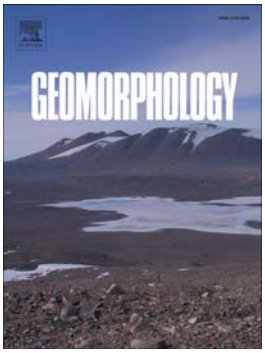

Ice cliff dynamics in the Everest region of the Central Himalaya

C. Scott Watson, Duncan J. Quincey, Jonathan L. Carrivick, Mark W. Smith

PII: S0169-555X(16)30733-4
DOI: doi: 10.1016/j.geomorph.2016.11.017
Reference: GEOMOR 5839

To appear in: *Geomorphology*

Received date: 16 August 2016
Revised date: 21 October 2016
Accepted date: 17 November 2016

Please cite this article as: Scott Watson, C., Quincey, Duncan J., Carrivick, Jonathan L., Smith, Mark W., Ice cliff dynamics in the Everest region of the Central Himalaya, *Geomorphology* (2016), doi: 10.1016/j.geomorph.2016.11.017

Ice cliff dynamics in the Everest region of the Central Himalaya

C. Scott Watson[1], Duncan J. Quincey[1], Jonathan L. Carrivick[1], Mark W. Smith[1]

1. School of Geography and water@leeds, University of Leeds, Leeds, LS2 9JT, UK

Correspondence to: C. S. Watson (scott@rockyglaciers.co.uk)

Abstract

The importance of ice cliffs for glacier-scale ablation on debris-covered glaciers is now widely recognised. However, a paucity of data exists to describe the spatio-temporal distribution of ice cliffs. In this study we analysed the position and geometry of 8,229 ice cliffs and 5,582 supraglacial ponds on 14 glaciers in the Everest region between 2000 and 2015. We observed notable ice cliff and pond spatial coincidence. On average across our study glaciers, 77 % of supraglacial pond area was associated with an adjacent ice cliff, and 49 % of ice cliffs featured an adjacent supraglacial pond. The spatial density of ice cliffs was not directly related to glacier velocity, but did peak within zones of active ice. Furthermore, we found that ice cliff density was glacier-specific, temporally variable, and was positively correlated with surface lowering and decreasing debris thickness for individual glaciers. Ice cliffs predominantly had a north-facing (commonly north-westerly) aspect, which was independent of glacier flow direction, thereby signifying a strong solar radiation control on cliff evolution. Independent field observations indicated that cliff morphology was related to aspect, local debris thickness, and presence of a supraglacial pond, and highlighted the importance of surface runnel formation, which acts as a preferential pathway for meltwater and debris fluxes. Overall, by coupling remote sensing and in-situ observations it has been possible to capture local and glacier-scale ice cliff dynamics across 14 glaciers over the past ~15 years, which is necessary if explicit parameterisation of ice cliffs in dynamic glacier models is to be achieved.

1. Introduction

A negative glacier mass balance regime prevails across the central and eastern Himalaya (e.g. Bolch et al., 2011; Bolch et al., 2012; Kaab et al., 2012; Nuimura et al., 2012; Kaab et al. 2015), and this is expected to continue under projected climate change (Chaturvedi et al., 2014; Zhao et al., 2014). This mass loss will lead to increasingly seasonal and declining water resources towards the end of the century (Lutz et al., 2014; Shea and Immerzeel, 2016; Soncini et al., 2016). Additionally, as proglacial lakes become established during deglaciation, assessments of glacial lake outburst flood hazards will become increasingly pertinent (Benn et al., 2012; Carrivick and Tweed, 2013).

Heavily debris-covered glaciers predominantly respond to negative glacier mass balance regimes via surface lowering, rather than by up-valley retreat of a glacier terminus (Scherler et al., 2011; Benn et al., 2012; Thakuri et al., 2014; Racoviteanu et al., 2015). Spatio-temporally heterogeneous debris-cover (Zhang et al., 2011; Nicholson and Benn, 2013) controls patterns of melt by locally insulating the glacier where debris exceeds a critical thickness, which is typically just a few centimetres (Östrem, 1959; Mattson et al., 1993; Nicholson and Benn, 2006). This means that maximum debris-covered Himalayan glacier surface lowering rates are most commonly found in the mid and upper parts of this debris-covered area because debris thickness generally decreases up-glacier (Nakawo et al., 1999). However, whilst considerable local-scale heterogeneity in supraglacial debris and other supraglacial features such as ponds and ice cliffs has been acknowledged (e.g. Immerzeel et al., 2014; Pellicciotti et al., 2015; Ye et al., 2015), a full spatio-temporal analysis of these supraglacial features has yet to be made.

A quantitative assessment of the evolution of supraglacial parts of Himalayan glacier systems is urgently required because diminishing ice surface gradients and consequently reduced

driving stress of debris-covered glaciers creates preferential conditions for supraglacial pond formation and expansion (Scherler et al., 2011; Benn et al., 2012). Indeed, several authors have documented a net increase in supraglacial pond area over recent decades (e.g. Gardelle et al. 2011; Nie et al. 2013; Wang et al. 2015; Watson et al., 2016). These supraglacial ponds can efficiently absorb and transmit thermal energy to adjacent ice cliffs (Sakai et al., 2000; Miles et al., 2016), and promote cliff calving rates of tens of metres per year (Table 1) (Benn et al., 2001). The resultant enhanced ice mass loss in shallow ice surface gradient zones can lead to a positive feedback cycle that may ultimately produce large glacial lakes (Reynolds, 2000; Bolch et al., 2011; Benn et al., 2012).

The aim of this study is to conduct a remote sensing analysis investigating the spatio-temporal dynamics of ice cliffs in the Everest region, which is informed by a summary of the existing ice cliff literature. Specifically we investigate: (1) the spatio-temporal distribution and aspect of ice cliffs; (2) the spatial coincidence of ice cliffs and supraglacial ponds; (3) associations between ice cliffs, glacier surface lowering, and debris-cover; (4) strategies for monitoring ice cliff evolution.

2. Previous work

2.1 Ice cliff and supraglacial pond inclusion into modelling studies

Quantifying ice cliff and supraglacial pond dynamics is important because studies modelling future glacier evolution do not fully incorporate these ice ablation processes (e.g. Rowan et al., 2015; Shea et al., 2015; Soncini et al., 2016). Douglas et al. (2016) parameterise ice cliffs as sources of locally enhanced melt by using an estimate of ice cliff distribution on the Khumbu Glacier but most studies calibrate glacier mass balance based on geodetic or previously-published estimates and thus account for the role of ice cliffs and ponds implicitly, meaning changes in their distribution, occurrence, and feedbacks are not represented.

Furthermore, estimates of glacier volume loss from different modelling studies using the same climatic scenarios are not consistent. For example, Shea et al. (2015) estimated a 84 % mean decrease in glacier volume for the Everest region to 2100 under an RCP4.5 scenario. For the Khumbu Glacier, Rowan et al. (2015) predict a volume loss of 8 to 10 %, whereas Soncini et al. (2016) predict 54 %, and Douglas et al. (2016) predict 72-75 %. Therefore, an improved process-based understanding of the surface dynamics of heavily debris-covered Himalayan glaciers would help refine model parameterisation.

2.2 Observations of ice cliff retreat

Direct observations of ice cliff retreat are spatially and temporally limited, but nonetheless demonstrate their importance for ablation on debris-covered glaciers (Table 1). Ablation stake measurements have supported numerical models of cliff evolution and quantification of ice cliff importance relative to sub-debris melt (e.g. Han et al., 2010; Reid and Brock, 2014; Steiner et al., 2015; Buri et al., 2016). Buri et al (2016) estimated that total ice cliff melt was 13 times higher than sub-debris melt in the Langtang region. Similarly, recent studies using multi-temporal digital elevation model (DEM) differencing have revealed high rates of localised surface lowering around ice cliffs and supraglacial ponds (Immerzeel et al., 2014; Pellicciotti et al., 2015; Thompson et al., 2016). For the Ngozumpa Glacier in the Everest region, Thompson et al. (2016) partitioned the observed surface lowering from fine-resolution DEMs of difference into respective contributions from ice cliffs, supraglacial ponds, and sub-debris melt. Here, cliffs covered ~ 5% of the debris-covered area but contributed ~ 40 % to observed surface lowering. Additionally, the majority of cliffs were north-facing, similar to the observations of Sakai et al. (2002) on the southerly flowing Lirung and Khumbu glaciers.

2.3 Ice cliff energy balance

Little is known about the relationship between radiation fluxes and cliff formation, persistence, and decay. A higher solar radiation receipt on south-facing cliffs is expected to cause their rapid decay and burial under debris following progressive slope angle lowering, which may explain why few south-facing cliffs are observed (Sakai et al., 2002). In contrast, ice cliff persistence is likely to be favoured on shaded north-facing slopes (Sakai et al., 2002; Steiner et al., 2015). The longwave radiation component of surface energy balance on heavily debris-covered glaciers was shown to be large by Steiner et al. (2015) and Buri et al. (2016) due to emissions from surrounding debris mounds adjacent to the base of ice cliffs. This is due to the debris-cover reaching high temperatures during the day, in contrast to clean ice (Nicholson and Benn, 2006; Steiner et al., 2015). On north-facing cliffs, a high longwave radiation input at the cliff base and low direct solar radiation input at the cliff top appears to maintain a steep cliff angle, favouring cliff persistence (Sakai et al., 2002). However, the monsoon dominated melt season of the central and eastern Himalaya complicates the energy balance due to influence of cloud cover (Sakai et al., 1998; Nicholson and Benn, 2013), which reduces the direct shortwave radiative flux but also reduces ambient temperature decline through the night (Steiner and Pellicciotti, 2016), potentially prolonging cliff melt.

Table 1. Observations of ice cliff retreat rates and characteristics on debris-covered glaciers

Reference	Location	Typical cliff melt rates (cm d^{-1}) M – modelled, O – Observed	Summary
Brun et al. (2016)	Lirung Glacier, Nepal	Monsoon: 3.8 – 3.1 O Post-monsoon: 1.0 O	• Calculated ice cliff volume losses by comparing five ice cliff faces over a year. The study cliffs were north-facing.
Buri et al. (2016)	Lirung Glacier, Nepal	Pre-monsoon: 1.2 – 8.6 M Monsoon: 0.9 – 7.9 M Post monsoon: 0.6 – 4.7 M	• Incoming longwave radiation was higher than the total incoming shortwave flux, due to radiation emitted by the surrounding terrain • Two cliffs occupied 0.09 % of the debris-covered area and accounted for 1.23 % of modelled total glacier melt

Steiner et al. (2015)	Lirung Glacier, Nepal	Pre-monsoon: 3.3 – 8.6 O Post- Monsoon: 0.2 – 1.3 O	• High spatial and temporal variability in cliff melt was observed • The role of local topography for cliff shading and increasing longwave radiation fluxes was an important consideration
Juen et al. (2014)	Koxkar Glacier, China		• Ice cliffs occupied 1.7 % of the debris-covered area and accounted for 12 % of the sub-debris ablation and 2.5 % of the total glacier ablation
Reid and Brock (2014)	Miage Glacier, Italy	5.9 – 8.1 O	• Mapped cliffs occupied ~ 1.3 % of the debris-covered area and accounted for ~ 7.4 % of modelled total ablation
Thompson et al. (2012)	Ngozumpa Glacier, Nepal		• Retreat rates of 20–50 m a^{-1} (2008–2010) of a cliff beside Spillway Lake were attributed to ice cliff calving
Han et al. (2010)	Koxkar Glacier, China	3 – 10 O	• 38 cliffs observed • Cliffs accounted for ~ 7.3 % of modelled debris-covered area runoff • There was a strong correlation between backwasting rate and daily mean temperature (R^2 = 0.84) • Shortwave radiation was the most important energy flux for cliff ablation
Rohl (2006)	Tasman Glacier, New Zealand	10 – 30 O (thermal undercutting)	• A mean notch formation rate of 15 cm d^{-1} was observed during the summer • A mean calving rate of 34 m a^{-1} was observed
Sakai et al. (2002)	Lirung & Khumbu Glaciers, Nepal		• Mapped cliffs occupied ~ 2.6 % of Khumbu Glacier debris-covered area. • Cliffs accounted for ~20 % of the debris-covered area ablation • North-facing cliffs were most common
Benn et al. (2001)	Ngozumpa Glacier, Nepal	Post Monsoon: 3.0 – 4.5 O (13.7 – 14.9 m a^{-1})	• Calving retreat initiated on cliffs > 15 m high • Mean calving retreat rates were 31 – 52 m a^{-1} • Subaerial melting was 20 – 50 % of the calving retreat rate
Sakai et al. (1998)	Lirung Glacier, Nepal	Monsoon: 7.2 O	• Mapped cliffs occupied < 2 % of the debris-covered area and accounted for 69 % of modelled total ablation
Inoue and Yoshida (1980)	Khumbu Glacier, Nepal	Monsoon: Up to 4.5 O	• Solar radiation was found to be most important for cliff ablation. Calving cliffs were observed

3. Study area

The Everest region spans the Nepal/Tibet border in the central Himalaya (Fig.1). Warming temperatures and reduced precipitation (Yang et al., 2006; Shrestha and Aryal, 2011; Yang et al., 2011; Salerno et al., 2015) have resulted in a widespread negative mass balance regime

(Bolch et al., 2008; Bolch et al., 2011; Benn et al., 2012; Ye et al., 2015) (Table 2). In this study, we focus on the debris-covered zones of 14 glaciers (Fig. 1). These glaciers range in size, predominant flow direction and in mass balance, and are amongst the highest altitude glaciers in the world (Table 2). Additionally, we use observations of ice cliffs on the Khumbu Glacier photographed during field campaigns in October/ November 2015 and May 2016 to investigate cliff morphology and fine-scale melt processes.

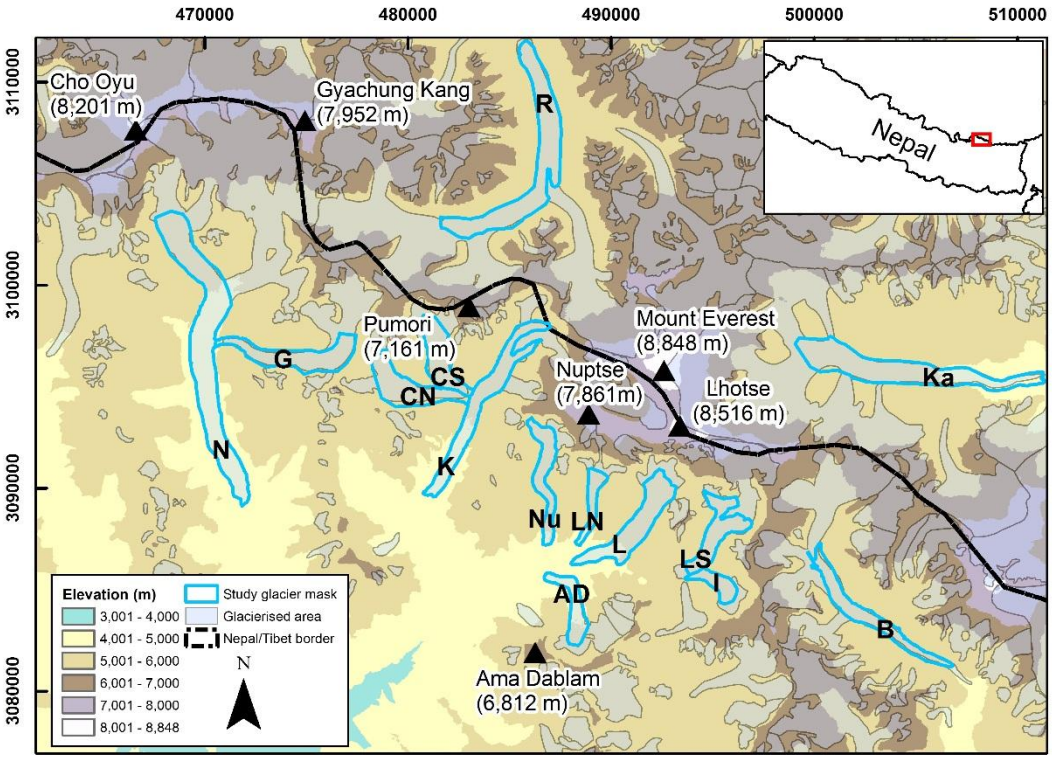

Figure 1. Study glaciers in the Everest region of Nepal/ Tibet. The study masks broadly represent the debris-covered area of each glacier. AD – Ama Dablam Glacier, B – Barun Glacier, CN – Changri Nup Glacier, CS – Changri Shar Glacier, G – Gaunara Glacier, I – Imja Glacier, Ka – Kangshung Glacier, K – Khumbu Glacier, L – Lhotse Glacier, LN – Lhotse Nup Glacier, LS - Lhotse Shar Glacier, N- Ngozumpa Glacier, Nu – Nuptse Glacier, and R - Rongbuk Glacier. Grid is UTM zone 45N

Table 2. Study glacier section characteristics

Glacier	Area (km^2)[1]	Length (km) [1]	Min – max elevation (range) (m) [1]	Gradient (°) [1]	Mean flow direction (°) [1]	Glacier Geodetic mass balance estimate (m.w.e. a^{-1})

Ama Dablam[2]	2.29	4.44	4,769 – 5,084 (315)	1.6	335	-0.29 ± 0.08*
Barun	3.89	9.17	5,018 – 5,453 (435)	1.5	129	-
Changri Nup[2]	4.62	5.75	5,057 – 5,540 (483)	1.6	118	-0.28 ± 0.08*
Changri Shar[2]	2.75	4.84	5,074 – 5,436 (362)	1.6	149	-0.28 ± 0.08*
Gaunara[2]	4.33	7.70	4,983 – 5,432 (449)	1.6	266	-
Imja	1.18	2.56	5,023 – 5,187 (164)	1.6	305	-0.50 ± 0.09*
Kangshung	10.0	12.1	4,586 – 5,377 (791)	1.6	94	-
Khumbu[2]	6.54	10.9	4,856 – 5,446 (590)	1.6	215	-0.27 ± 0.08*
Lhotse	5.76	6.73	4,815 – 5,245 (430)	1.6	230	-0.26 ± 0.08*
Lhotse Nup[2]	1.40	3.88	4,954 – 5,210 (256)	1.6	197	-0.18 ± 0.07*
Lhotse Shar	3.03	4.05	5,008 – 5,329 (321)	1.6	229	-0.50 ± 0.09*
Ngozumpa[2]	15.1	15.8	4,668 – 5,241 (573)	1.5	165	-
Nuptse[2]	3.04	6.19	4,962 – 5,554 (592)	1.6	178	-0.25 ± 0.08*
Rongbuk[2]	8.83	13.0	5,174 – 5,526 (352)	1.5	24	-0.42 ± 0.27**

1. Statistics are calculated for the study glacier masks of each glacier, which broadly represent the debris-covered area of each glacier.
2. Indicates glaciers with velocity data.

* 1970 – 2007 from Bolch et al. (2011). Note that Lhotse Shar and Imja, and Changri Nup and Changri Shar glaciers are not separated by Bolch et al. (2011).
** 1974 – 2006 from Ye et al. (2015)

4. Datasets and methods

4.1 Ice cliff and supraglacial pond classification and analysis

True-colour orthorectified satellite imagery (< 2 m spatial resolution) of the Everest region was accessed through Google Earth Pro. Images from December 2000 to June 2015 provided multi-temporal coverage for most of our study glaciers (Fig. 2). The core imagery was selected based on a visual inspection of its quality (ice cliff contrast with the surrounding debris, snow cover, and presence of shadows) rather than acquisition date. Ice cliff presence is not seasonal in contrast to supraglacial ponds, which expand during the summer melt season. Glacier outlines were modified from the South Asia – East Randolph Glacier Inventory 5.0 (Pfeffer et al., 2014) to reflect the debris-covered area of each glacier, which were used as study masks. These masks excluded areas of heavily crevassed 'dirty-ice' where ice cliffs could not be clearly delineated, and areas of avalanche deposits or seasonal snow cover, both of which occurred at the debris to clean-ice transition. The study masks for the

Rongbuk and Kangshung glaciers stopped below the transition from debris-covered to clean-ice due to data availability, omitting ~4 km^2 and ~3 km^2 of debris-covered area respectively.

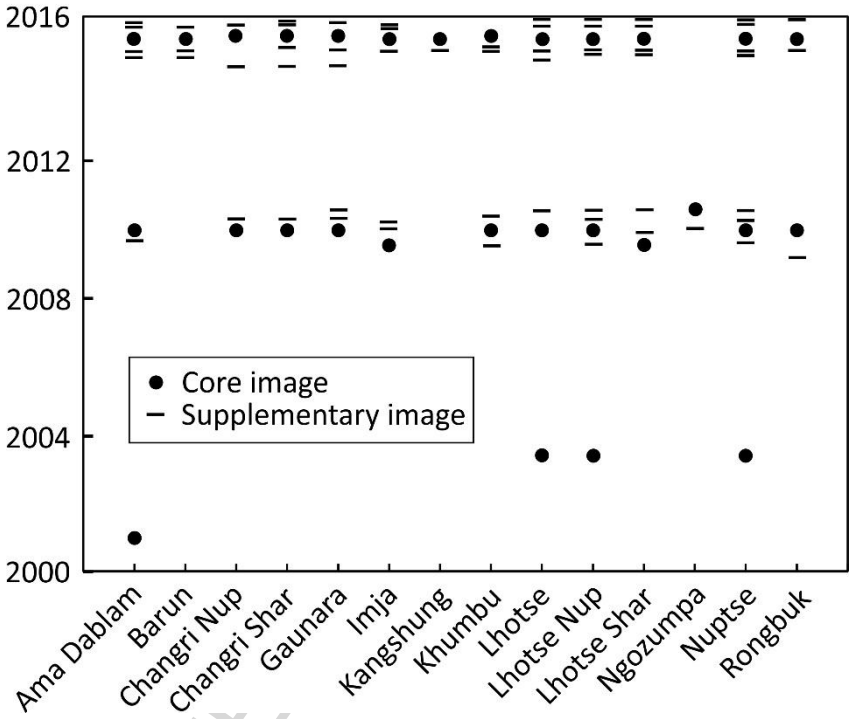

Figure 2. Temporal and spatial coverage of the satellite imagery used in this study. Ice cliffs were digitised on core images, using supplementary images for cross-referencing.

All ice cliffs and supraglacial ponds were manually delineated in Google Earth Pro by one operator and checked on independent days until no further edits were required. We define an ice cliff as any area of exposed ice, whether this is clean ice or dirty (i.e. with a thin layer of debris on the surface). Ice cliffs were digitised along the length of their top edge from left to right with the cliff facing outward (Fig. 3). Supplementary satellite imagery was used where available to cross-check the cliffs (Fig. 2) and a total of 8,229 cliffs and 5,582 supraglacial ponds were digitised (Supplementary Table 1).

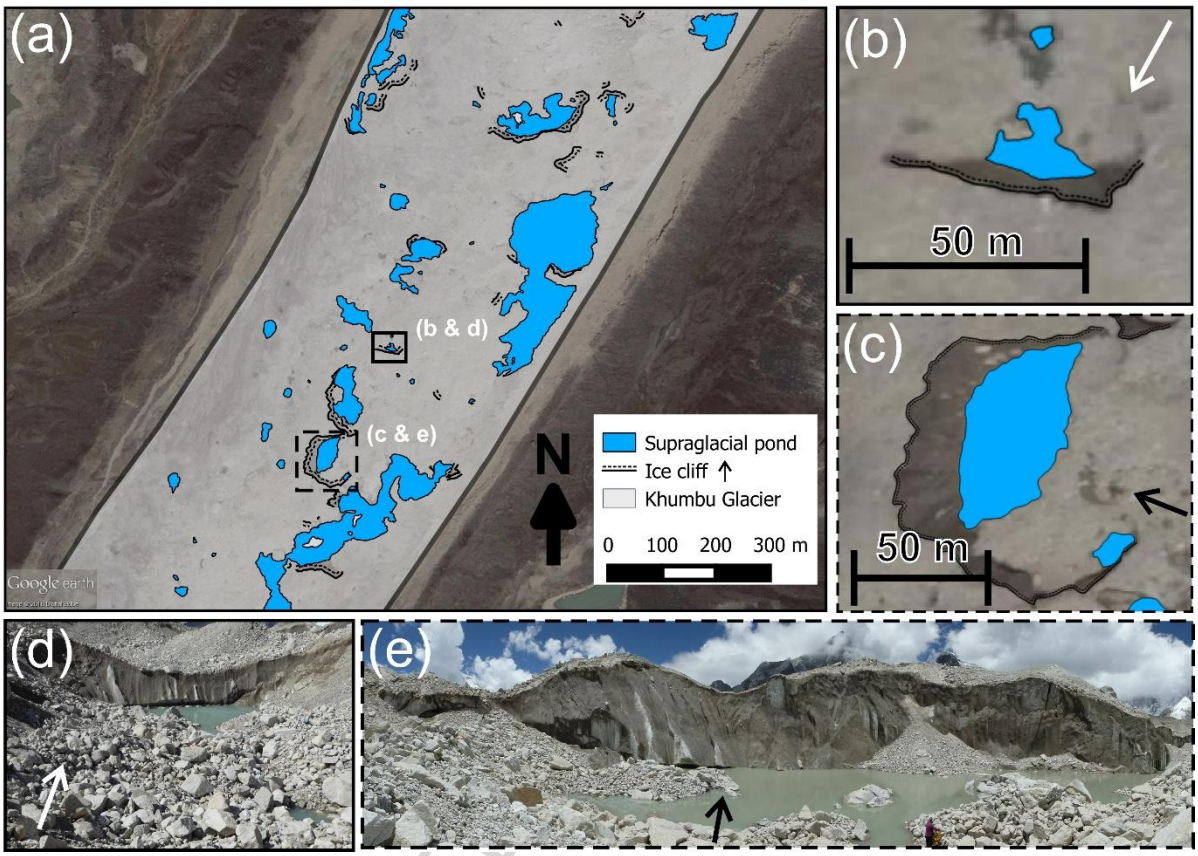

Figure 3. Ice cliffs and supraglacial ponds digitised on the Khumbu Glacier. (a) Digitised ice cliffs and supraglacial ponds overlaid on respective Google Earth imagery. Ice cliff aspect is indicated by the offset dotted line. (b) A north-facing cliff and pond, and (c) an easterly facing cliff and pond. Respective cliff photographs and viewing directions are shown in (d) and (e).

Glacier centrelines were automatically calculated in ArcGIS using the study masks and the 'Collapse Dual Lines to Centerline' tool (cf. Haritashya et al. 2015). Glacier centrelines were used to calculate glacier length and mean flow direction. Glacier surface gradients were calculated using the length and elevation change of the study masks. Ice cliffs were segmented by vertices in ArcGIS and the outward looking aspect of each segment was calculated. These segments were used in subsequent analysis to preserve the cliff-scale variation, rather than taking a mean across each cliff. Cliff length was summed per glacier and into 500 m distance bins, which started at the glacier terminus and accounted for

centreline curvature. We calculated cliff length per unit area as a cliff density metric, which is referred to herein as cliff density.

The spatial coincidence between ice cliffs and supraglacial ponds was assessed using a 30 m directional buffer from each cliff top edge. The buffer was used to extract ponds that intersected with the buffer polygon since cliff geometry and hence the distance between the cliff top edge and potential pond was unknown (Supplementary Fig. 1). Taking 30º as the debris angle of repose (Sakai et al., 1998) and a cliff height of 15.5 m (a mean from the Ngozumpa Glacier observed by Thompson et al. 2016), a theoretical pond would be at least 27 m from the top edge of the cliff. Furthermore, 15 m is suggested as the threshold for calving initiation (Benn et al., 2001) and hence should represent and approximate upper bound for steeply sloping cliff faces. The buffer size was also supported by our field-based and satellite observations.

4.1.1 Glacier surface elevation change and debris-thickness

We used surface elevation change data of glaciers in the Everest region (2000 to 2015) from King et al. (2016) and the modelled debris thickness data of Rounce et al. (2015) to assess relationships with ice cliff density. The surface lowering and debris thickness data had coverage for nine and seven glaciers respectively and both datasets were generated at 30 m resolution. King et al. (2016) derived surface lowering data through the subtraction of an 8 m resolution 2015 DEM (resampled to 30 m) generated and distributed by the Polar Geospatial Centre at the University of Minnesota, and the co-registered 30 m resolution 2000 Shuttle Radar Topographic Mission (SRTM) DEM version 3.0. The modelled debris-thickness data of Rounce et al. (2015) were derived using an energy balance model and Landsat 7 Enhanced Thematic Mapper Plus (ETM+) satellite imagery (2002 to 2009). Modelled debris thicknesses were comparable with field-based measurements in the region, although the approach is only suitable for determining thicknesses below 0.5 m and hence provides a

lower bound estimate (Foster et al., 2012; Rounce and McKinney, 2014). Notably however, ablation is negligible at debris thicknesses above 0.5 m (Mattson et al., 1993).

4.1.2 Glacier velocity

Glacier velocities were calculated by tracking surface features between a pair of TerraSAR-X images acquired approximately twelve months apart (18th January 2015 and 5th January 2016). We used a cross-correlation algorithm (Luckman et al., 2007) to identify displaced features using a pattern size (window) of 64 x 64 pixels within a search area of 128 x 128 pixels, equating to approximately 450 x 575 m and 900 x 1150 m on the ground respectively. Scene availability limited our analysis to nine of the fourteen studied glaciers (Table 2) but the density of matches on those nine glaciers was excellent given the abundance of surface features. Measured displacements were filtered to remove clear blunders and scaled to annual velocities using the time separation of the images. They were then projected onto a UTM grid at 8 m spatial resolution. We estimated the precision of the method to be approximately half a pixel and thus removed all data points < 3 m a^{-1} from our subsequent analysis.

4.1.3 Uncertainty assessment

Ice cliff length uncertainty is influenced by image resolution, operator ambiguity in the identification of a cliff, and operator digitisation of the cliff. In this study, we used fine-resolution imagery of comparable resolution where cliffs were clearly visible and one operator undertook all of the analysis. Therefore the latter process, cliff digitisation, is likely to be the main source of uncertainty. To assess the operator error in cliff digitisation, 60 cliffs were randomly selected in each of the core images and repeat digitised. No systematic bias was observed between images in this analysis suggesting that the operator was consistent throughout (Supplementary Fig. 2). The standard deviation of cliff differences ranged from

4.1 to 8.9 m, which we use as an indication of ice cliff delineation repeatability, although we are aware that potential omissions or commissions are not considered.

4.2 Field observations from the Khumbu Glacier

Six ice cliffs were photographed during field campaigns on the Khumbu Glacier (Oct – Nov 2015 and May 2016) and whilst this was initially to ground-truth the remotely-sensed observation the images also revealed and characterised the variable morphology of cliffs. In particular we explored ice cliff coincidence with supraglacial ponds, cliff shape, meltwater generation and drainage patterns, and evidence of evolutionary characteristics.

5. Results

5.1 Ice cliff and supraglacial pond density and spatial coincidence

The density of supraglacial ponds (ponded area as a percentage of glacier area) and ice cliffs (cliff length per glacier area) was variable across our study glaciers and through time (Fig. 4). The highest cliff densities were on Lhotse Shar and Imja glaciers with 7.4 and 7.1 mm/m^2 respectively. Similarly, the greatest cliff density changes were on Lhotse Shar and Imja glaciers, which both featured a notable decrease in ice cliffs over the study period. When ranked, a high cliff density did not necessarily equate to high pond density. Cliff density was unrelated to glacier gradient, which displayed little inter-glacier variability (1.5 - 1.6°), or mean glacier flow direction. Bolch et al. (2011) found Lhotse Shar/ Imja Glacier to have the most negative mass balance reported for our study glaciers (-0.50 ± 0.9 m.w.e. a^{-1}), and Lhotse Nup to have the least negative (0.18 ± 0.07 m.w.e. a^{-1}) (Table 2). Similarly, we found these glaciers to have the highest and lowest cliff densities respectively (Fig. 4b).

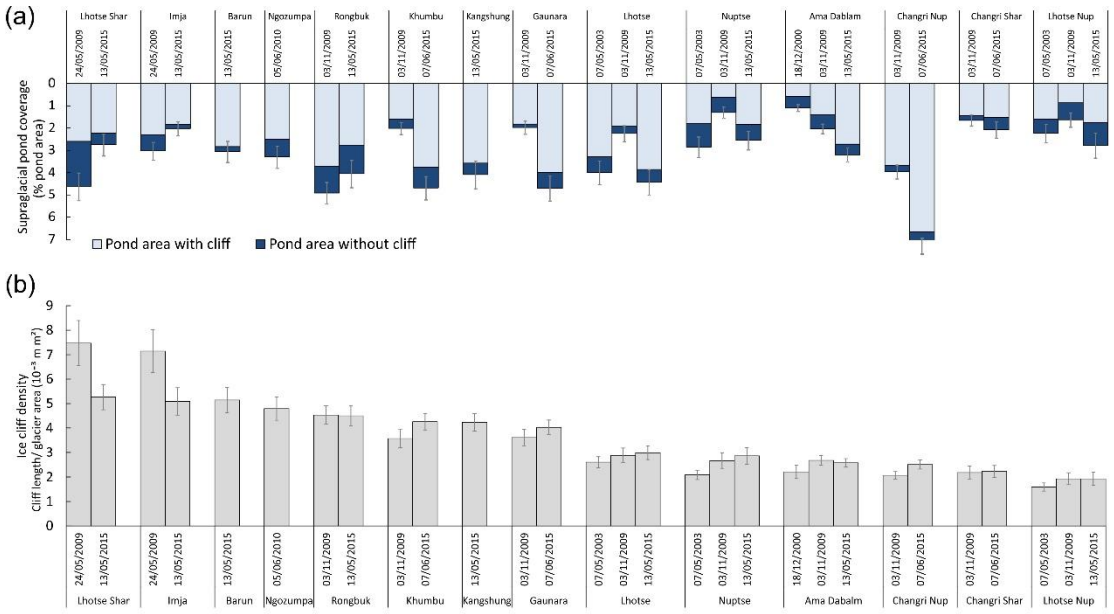

Figure 4. (a) Supraglacial pond coverage per glacier for ponds with and without associated ice cliffs; lake area at the termini of Lhotse Shar, Imja, Ngozumpa and Rongbuk glaciers is excluded for clarity and error bars represent a ± 1 m pond boundary uncertainty. (b) Ice cliff density ranked high to low by glacier. Error bars represent the standard deviation of cliff length differences from the repeat digitisation analysis (Supplementary Fig. 2).

The area of supraglacial ponds with a coincident ice cliff far exceeded the area of those without (Fig. 4a). Ponds accounted for between 1 % (Ama Dablam 2000) and 7 % (Changri Nup 2015) of glacier area, and between 43 % (Nuptse 2009) and 95 % (Changri Nup 2015) of pond area had an adjacent ice cliff, with a mean of 77 % (Fig. 4a). On average across our study glaciers, 51 % of the total number of ponds had a coincident ice cliff and larger ponds were more likely to feature an ice cliff (Table 3, Supplementary Figure 3). Similarly, on average 49 % of ice cliffs had a coincident pond. Generally, longer cliffs were most likely to have a coincident pond and larger ponds were most likely to have a coincident cliff (Fig. 5, Supplementary Figure 3). Notably (with the exception of Ama Dablam Glacier with longer cliffs) cliffs 20 – 40 m in length were most frequent across our study glaciers.

Table 3. Summary data of the spatial coincidence between ice cliffs and supraglacial ponds

Ice cliffs with a supraglacial pond	49 %
Ice cliffs without a supraglacial pond	51 %

Supraglacial ponds with an ice cliff	51 %
Supraglacial ponds without an ice cliff	49 %

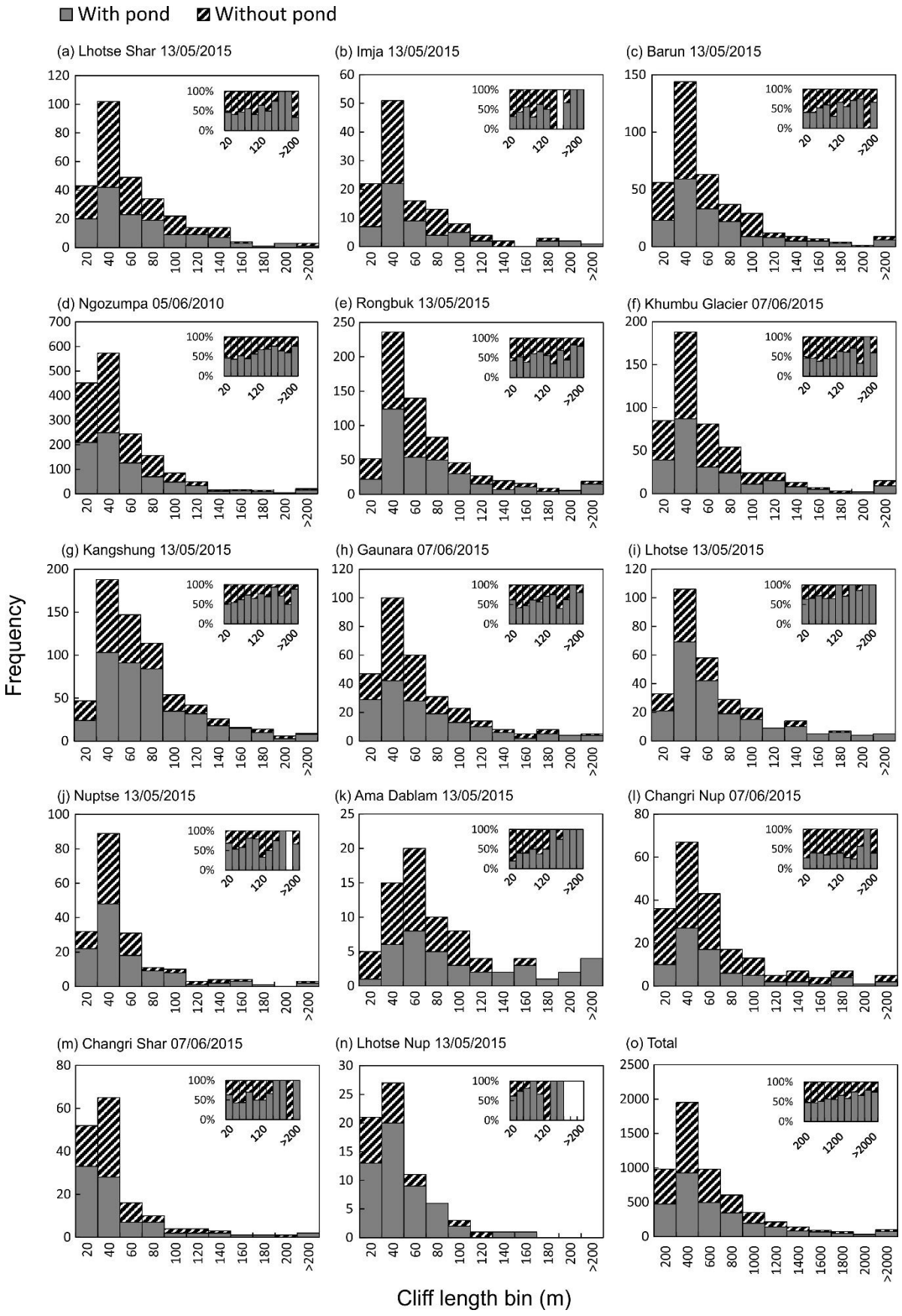

Figure 5. Size distribution of ice cliffs and coincidence with supraglacial ponds, for the most recent time period for each glacier. Insets show the same data as a percentage distribution.

5.2 Ice cliff aspect

Ice cliffs were shown to be strongly dependent on aspect and strongly independent of glacier flow direction (Figure 6). North-facing ice cliffs prevailed, although a slight deviation was observed on Kangshung and Barun glaciers, which flow in an easterly direction and predominantly featured north easterly facing cliffs. In contrast, cliffs mostly faced northwest on the remaining study glaciers despite a range of flow directions. The maximum intra-glacier change in cliff aspect (80°) was on Lhotse Shar Glacier (2009 to 2015).

Temporal changes in cliff aspect were variable by glacier for both the magnitude and direction of change (Fig. 6). Several glaciers displayed little temporal change in the overall mean cliff aspect (< 20°) e.g. Gaunara, Changi Nup, Changri Shar, and Lhotse Nup glaciers, whereas others displayed large changes (≥ 20°) e.g. Lhotse Shar, Imja, Rongbuk, Khumbu, Nuptse, Ama Dablam and Lhotse glaciers (Fig. 6). Additionally, we note that several glaciers exhibited a decline in north-facing cliffs over our study period. Whether these are recent or long-standing changes is not clear because of the limited temporal resolution of our data.

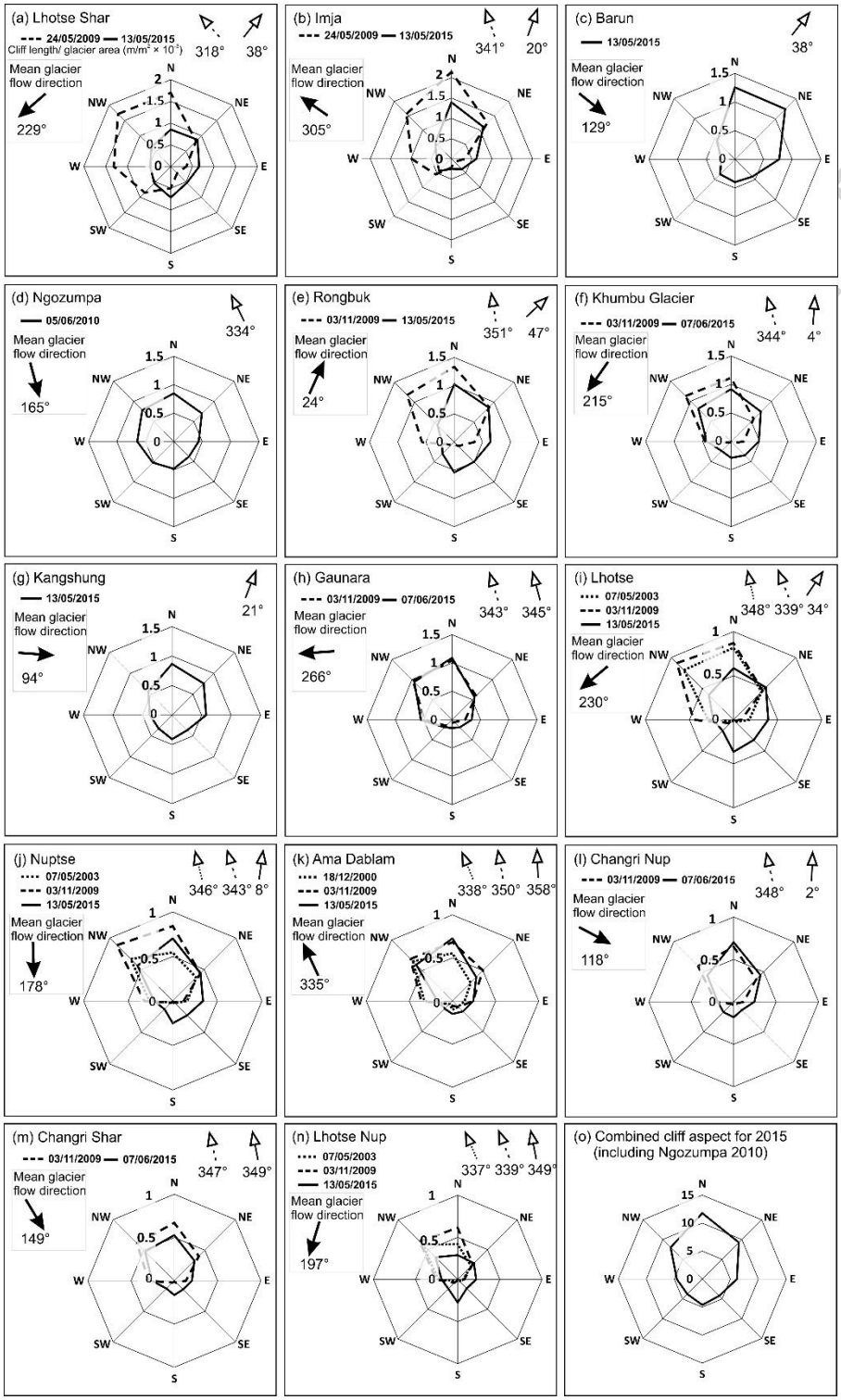

Figure 6. Aspect roses for each glacier showing cliff length per glacier area (m/ $m^2 \times 10^{-3}$). Arrows indicate the mean cliff aspect for each time period. Note the different scale ranges.

5.3 Spatial distribution of ice cliffs

Ice cliff density generally increased up-glacier from the terminus and peaked in the upper region of the study masks (Fig. 7), which were areas below peak velocity, and of thin or decreasing debris-thickness (Fig. 8). However, seven of our study glaciers displayed an increasing trend with distance from the terminus, followed by a decrease into the transition zone between clean and debris-covered ice (e.g. Lhotse Shar, Barun, Ngozumpa, Khumbu, Lhotse, Nuptse, and Lhotse Nup). Temporal change in cliff length was generally evident along the full length of each study glacier, even for glaciers with no or slow flow around their termini (e.g. Rongbuk, Khumbu, Gaunara, Nuptse, Changri Nup and Lhotse Nup glaciers). We did not observe a relationship between distance up-glacier from the terminus and the distribution of ice cliff lengths. Overall, ice cliff development and persistence appears to be independent of glacier surface velocity although cliff density did peak within zones of active ice.

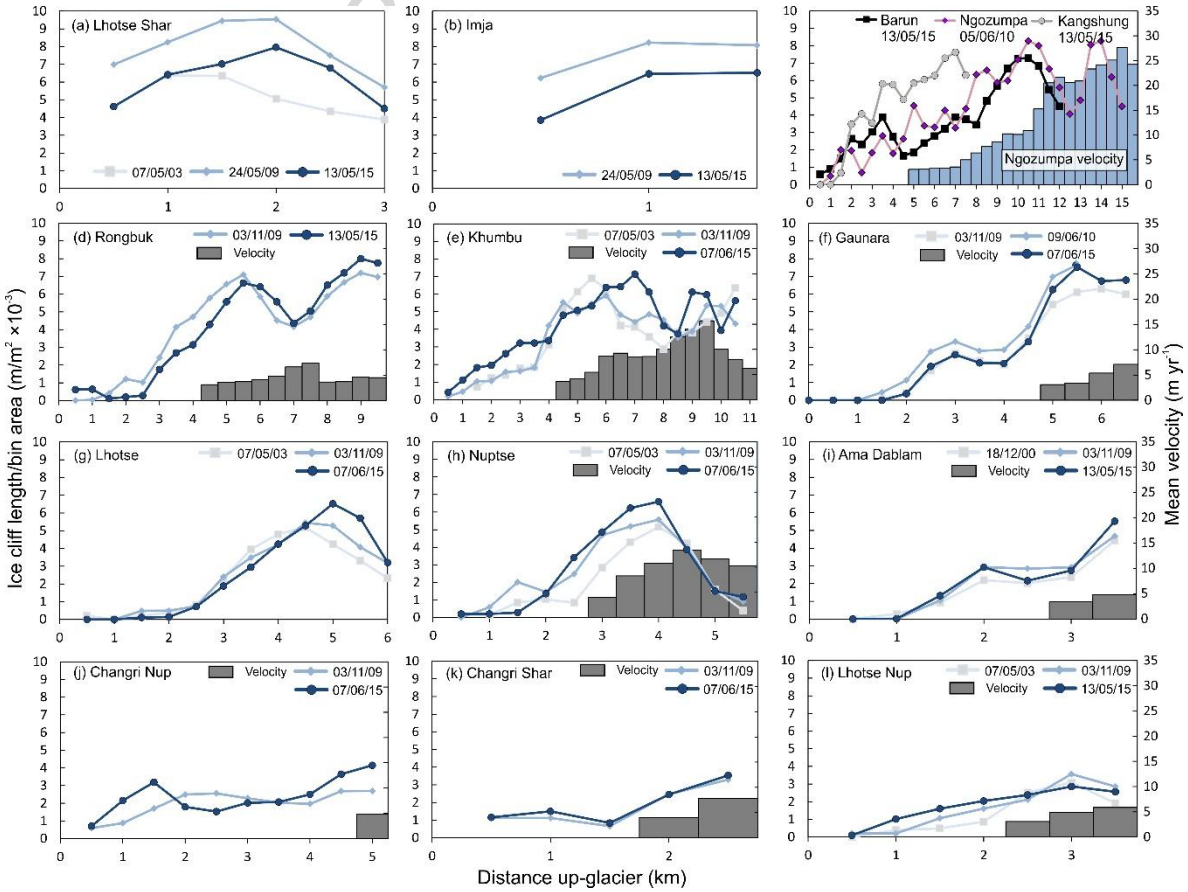

Figure 7. Ice cliff density with distance up-glacier from the terminus. The data represent a two-period moving average over 500 m distance bins. Velocity data are shown for the Ngozumpa, Rongbuk, Khumbu, Gaurana, Nuptse, Ama Dablam, Changri Nup, Changri Shar, and Lhotse Nup glaciers. The date format is dd/mm/yy.

There were clear relationships between cliff density, surface lowering, and modelled debris thickness, within and between each glacier (Figure 8). Debris thickness decreased up-glacier from the terminus from a maximum depth not exceeding 0.6 m (noting the methodological limitation). Surface lowering rates increased up-glacier from the terminus before plateauing and in some cases decreased again towards the up-glacier end of the study mask. Cliff density increased from the terminus alongside surface lowering and we observed statistically significant correlations for this rising limb (e.g. blue line Fig.8 a, b, c, f, i). After surface lowering plateaued, cliff density also plateaued or began to decrease (Fig. 8 a, b, c, f). In contrast to this prevailing trend, Lhotse Shar and Imja Glaciers featured high initial surface lowering rates at the terminus, which decreased up-glacier (Fig. 8g, h)

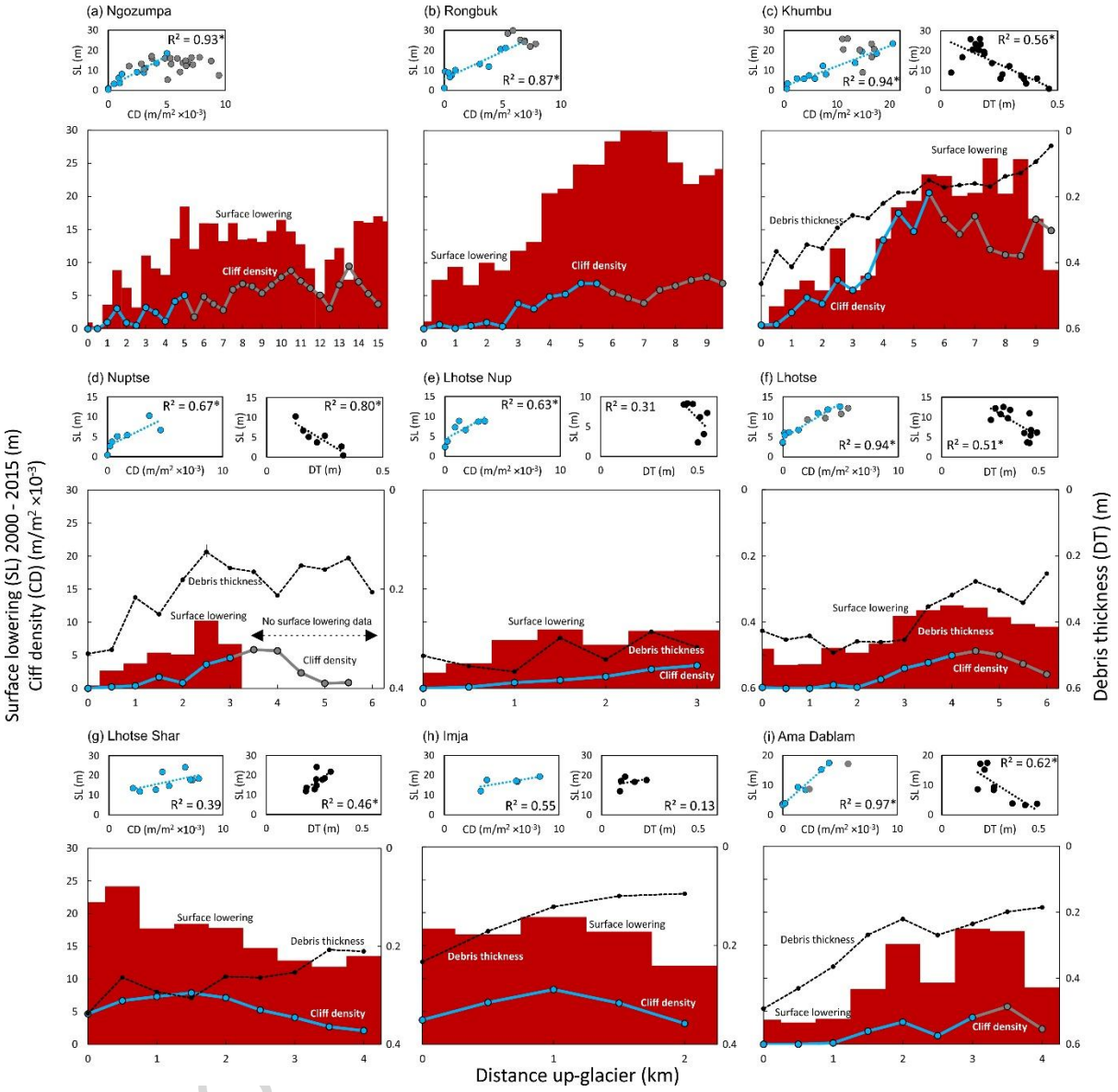

Figure 8. Spatial distribution of mean surface lowering, mean cliff density, and mean debris thickness with distance up-glacier from the terminus in 500 m distance bins. Correlations are shown for cliff density and surface lowering (light blue), and debris thickness and surface lowering (black). '*' indicates statistical significance ($P < 0.05$). Debris thickness data were unavailable for Ngozumpa and Rongbuk glaciers.

6. Discussion

The importance of ice cliffs for ablation on heavily debris-covered glaciers has long been suggested (e.g. Inoue and Yoshida, 1980). However, spatial and temporal measurements of ice cliff melt and calving retreat are exceptionally limited, owing to hazardous access to the cliff faces and the non-trivial task of working on debris-covered glaciers. Nonetheless,

explicit parametrisation of ice cliff processes within ice dynamics models for projecting glacier evolution requires data on (1) ice cliff distribution and characteristics at a glacier-scale, and (2) multi-temporal cliff-scale observations of their 3D evolution. Our results address (1), revealing ice cliff distribution, short-term temporal change, and relationships with glacier surface dynamics in the Everest region. Using our remote sensing analysis and observations of ice cliffs on the Khumbu Glacier, we are able to propose strategies for addressing (2).

6.1 Ice cliff dynamics

Ice cliffs are observed to form on debris-covered glaciers through two main processes: (1) steepening of slopes beyond the gradient required to hold debris (Sakai et al., 1998; Benn et al., 2007), and (2) the collapse of englacial conduits or voids creating a surface depression bordered by an arc of exposed ice (Kirkbride, 1993). To assess ice cliff dynamics at a glacier-scale we consider the spatial density of ice cliffs; spatial coincidence of ice cliffs with supraglacial ponds; cliff aspect; spatial distribution and relationship with glacier velocity, surface lowering and debris-cover; and cliff-scale morphology.

6.1.1 Ice cliff density

Ice cliffs were most prevalent on Lhotse Shar Glacier, and least on Lhotse Nup Glacier (Fig. 4), which featured the most and least negative mass balance regimes respectively (Table 2). High cliff density, or the proportion of bare ice on the debris-covered surface, is expected to be associated with high glacier surface lowering, as suggested by DEMs of difference (e.g. Immerzeel et al. 2014; Pellicciotti et al. 2015). This situation reflects ‘regime 2’ glaciers described by Benn et al. (2012) where ice flux down-glacier is exceeded by mass loss in the ablation zone where ice cliffs and ponds prevail. However, comparisons between published glacier mass balance data and cliff density patterns from the current study are complicated

since the available mass balance estimates either have a temporal interval greater than a decade or, conversely, shorter time periods feature high uncertainty (Bolch et al., 2011; Nuimura et al., 2012).

The ice cliff dataset presented in this study spans only the most recent decade and historic ice cliff distribution is unknown, although we note for the Khumbu Glacier that contemporary ice cliff distribution is visually comparable to that mapped in the late 1970s by Iwata et al. (1980). A fine-resolution contemporary DEM of difference is currently lacking for the Everest region, which would allow a more robust assessment of the association between ice cliffs and surface elevation change at a glacier scale (e.g. Thompson et al. 2016).

6.1.2 Spatial coincidence of ice cliffs and supraglacial ponds

Supraglacial ponds covered between 1 % (Ama Dablam 2000) and 7 % (Changri Nup 2015) of glacier area (Fig. 4a). The percentage of pond area with a coincident ice cliff ranged from 43 % (Nuptse 2009) to 95 % (Changri Nup 2015). Lower pond-cliff coincidence is expected for non-monsoonal time periods (e.g. Nuptse November 2009), since ponds are expected to attain their maximum size in the preceding summer melt season (e.g. Watson et al. 2016) and ice-contact ponds are most seasonal (Benn et al., 2001). Across our study glaciers, 30 to 76 % of ice cliffs featured a coincident pond, with a mean of 49 %. Cliffs of all sizes were spatially coincident with supraglacial ponds, although this coincidence was generally greater for longer cliffs (Fig. 5). Overall, the observed high pond-cliff coincidence supports the formation mechanism hypothesis of ice cliffs by englacial conduit or void collapse and the creation of a hollow in which a pond can develop (Kirkbride, 1993). A similarly high coincidence was reported by Thompson et al. (2016) on the Ngozumpa Glacier where 75 % of cliffs bordered a pond.

Increasing supraglacial water storage in the region (Watson et al., 2016) promoted by low gradient debris-covered tongues (e.g. Reynolds, 2000; Quincey et al., 2007; Salerno et al., 2012) suggests that the importance of the observed cliff-pond interaction will become increasingly pertinent in coming decades, especially if there is a trajectory towards calving retreat. The transition of cliffs from melt-driven to rapid calving retreat is likely to increase as ponds coalesce to exceed the ~80 m fetch threshold proposed for calving initiation (Sakai et al., 2009), which can increase cliff recession threefold (Benn et al., 2001). We observed calving events on ice cliffs with ponds smaller than this threshold (e.g. Fig. 3e, 10f), where small calving events likely accompanied the thermal undercutting of the cliff face. Furthermore, seasonal expansion and drainage of supraglacial ponds transmits the absorbed thermal energy englacially, which can promote conduit collapse and subsequent cliff formation (Sakai et al., 2000; Miles et al., 2016), hence some consideration of how processes impact on and feedback to one another is also paramount for the accurate projection of glacier evolution.

6.1.3 Ice cliff aspect

Ice cliffs were observed to be predominantly north-facing across all 14 glaciers (Fig. 6). North-facing cliffs were found to prevail on the southerly flowing Lirung and Khumbu glaciers by Sakai et al. (2002), on the Koxkar Glacier by Han et al. (2010), and more recently on the Ngozumpa Glacier by Thompson et al. (2016). Our results demonstrate that this trend prevails throughout the Everest region of the Himalaya irrespective of glacier flow direction.

Our results support the prevailing hypothesis that south-facing cliffs may decay rapidly due to a high solar radiation receipt, hence explaining their reduced occurrence (Sakai et al., 2002). In contrast, north-facing cliffs may persist due to shading of the cliff face (Sakai et al., 2002; Steiner et al., 2015). Debris mounds on high-relief debris-covered glaciers emit a large

longwave radiation flux to the base of adjacent ice cliffs (Steiner et al., 2015; Buri et al., 2016). On north-facing cliffs this longwave radiation receipt could act to maintain a steep slope angle and hence promote persistence (Sakai et al., 2002). In contrast, high solar radiation receipt on south-facing cliffs promotes a lowering of the cliff slope and hence burial by debris once below a critical angle of ~30º (Sakai et al., 1998; Benn et al., 2007). However, increased temporal resolution is required to track the lifespan of individual cliffs and reveal the timescale of south-facing cliff decay, which could occur within a year given the high retreat rates observed (Table 1).

6.1.4 Spatial distribution of ice cliffs

We observed a generally increasing trend of ice cliff density with distance from glacier termini and several glaciers displayed peak cliff occurrence in their upper reach, followed by a decreasing trend (Fig. 7). Velocity data for nine of our study glaciers showed an increasing trend up-glacier from stagnant lower reaches comparable to Quincey et al. (2009), though we did not observe a clear association between cliff occurrence and glacier velocity. The stagnant ice zones (i.e. those flowing at a rate lower than the noise in our data) ranged from 2.0 (Lhotse Nup) to 4.5 km (Gaunara & Ngozumpa) up-glacier from the respective termini. Ice cliffs were spatially and temporally variable in these slow-flowing regions, indicating that the glacier surface is still actively collapsing into conduits and promoting cliff formation (e.g. Gulley and Benn, 2007). Notable surface lowering here supports this observation and we reveal a statistically significant positive correlation between ice cliff density and surface lowering for six of the nine study glaciers with available data (blue line, Fig. 8a, b, c, d, f, i).

Available debris thickness data show a decreasing trend up-glacier (Rounce and McKinney, 2014) and we suggest that the plateau of surface lowering marks a transition from high to moderate influence of ice cliffs for ablation, relative to sub-debris melt (grey line in Fig. 8

and zone 2 to 3 in Fig. 9). Debris thickness is known to be locally heterogeneous but generally decreases up-glacier from a thickness of several metres at the terminus, indicating that the debris acts to reduce ablation across the majority of the debris-covered zone by insulating the ice beneath (Nakawo et al., 1986; Benn et al., 2012; Nicholson and Benn, 2013; Rounce and McKinney, 2014). Debris-thicknesses in Figure 8 do not exceed 0.6 m, which reflects a methodological limitation in model estimates (Foster et al., 2012; Rounce and McKinney, 2014). Nevertheless, the relative trend observed up-glacier matches that expected for a debris-covered glacier. Generally weaker correlations between debris thickness and cliff density lend support to cliff density having a larger influence over surface lowering on the lower tongues, although there is clearly an interaction between all three variables. The surface lowering associated with the prevalence of a thin debris layer further up-glacier increasingly masks the contribution of ice cliffs (Fig. 9), i.e. the two surface lowering signals cannot be separated. This observation is supported by Thompson et al (2016) who found an increasing importance of sub-debris melt and decreasing importance of ice cliff retreat with distance up the Ngozumpa Glacier, although data were only reported for the lower 6 km.

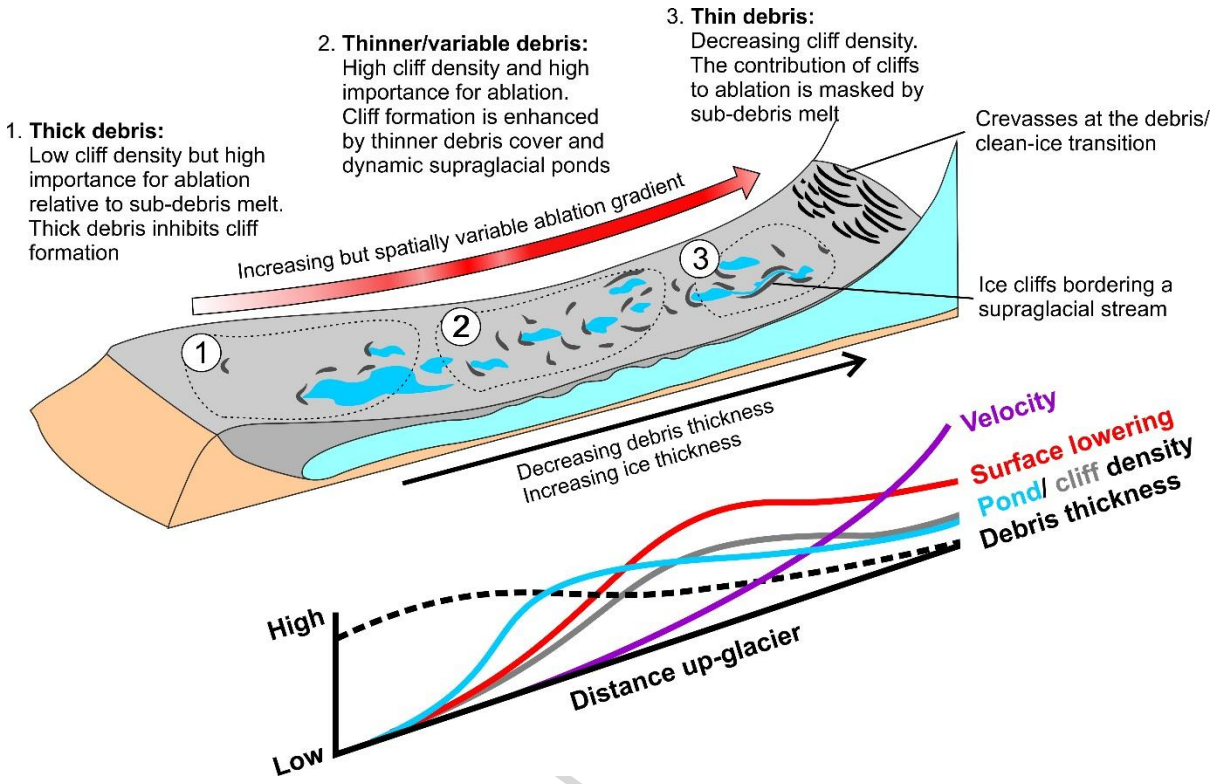

Figure 9. The interaction and associated ablation between ice cliffs, supraglacial ponds, and debris thickness on a debris-covered glacier.

The relationship between cliff density and surface lowering was not clear on Lhotse Nup Glacier or on the lake-calving Lhotse Shar and Imja glaciers (Fig. 8). These three glaciers were the smallest in our study. A relatively uniform high debris thickness (> 0.4 m) on Lhotse Nup Glacier likely inhibits cliff formation here since supraglacial pond coverage is similarly low (Fig. 4a). Several studies have identified highest rates of surface lowering at the terminus of the lake-calving Lhotse Shar Glacier (Bolch et al., 2011; Nuimura et al., 2012; Thakuri et al., 2016) comparable to our results (Fig. 8g). This trend contrasts with other glaciers in the region where highest rates are further up-glacier. Nuimura et al. (2012) hypothesised that reduced ice compression could be implicated in a reduction in emergence velocity, which contributes towards this high surface lowering signal at the terminus. Active flow along the length of Lhotse Shar Glacier also supports this hypothesis (Thakuri et al.,

2016). Similarly, a larger dataset of lake-calving glaciers analysed by King et al. (2016) also revealed high rates of terminus surface lowering.

6.2 Debris-covered glacier evolution

It is important to be able to characterise the interaction between ice cliffs, supraglacial ponds, debris thickness, and surface lowering when considering future glacier evolution, especially where the number of cliffs and ponds displays an increasing trend (Fig. 4) (Rowan et al., 2015; Watson et al., 2016). A temporal up-glacier migration in the occurrence of cliffs is not apparent in our relatively short dataset, yet might be expected to accompany predicted volume loss in the coming century. In practical terms, the observations of cliff density, spatial dynamics and relationships, and cliff aspect presented in this study could be used to inform a glacier-specific and spatial parameterisation of ice cliff ablation when combined with local observations of cliff retreat (Table 1). However, knowledge of respective cliff areas is still lacking unless corresponding DEMs are available. Additionally, even with corresponding DEMs, the surface topography of steep cliff faces is likely to be poorly represented (Kolecka, 2012). Therefore, investigating a relationship between cliff length and mean cliff height could improve the utility of remote-sensing observations, especially since we observe similar frequency distributions of cliff length for each of our study glaciers (Fig. 5). Here, cliffs between 21 and 40 m in length were most common. Relationships between surface lowering, cliff density, and debris thickness were apparent in this study using a 30 m resolution dataset. However, it is clear that an increased spatial coverage of fine-resolution DEM differencing (e.g. Thompson et al. 2016), combined with local-scale observations of retreat, is the best strategy to further investigate their spatial and temporal significance.

6.3 Strategies for monitoring cliff evolution

The remote sensing analysis presented in this study reveals planimetric ice cliff dynamics but does not represent the heterogeneity of ice cliff morphologies that we observed in the field. Our field observations indicate that an ablation gradient is likely to be present on crescentic cliffs, which span a range of aspects (Fig. 10). We identified meltwater runnel formation on several of these cliffs, which act as preferential pathways for meltwater and debris fluxes (falling debris and saturated debris flows). Runnel persistence is likely to be governed by the background rate of cliff melt, which determines the rate at which the runnel can incise, similar to the formation process of supraglacial streams (Hambrey, 1977), and the supply of meltwater and debris down the cliff face. Once established, the runnels create local topographic shading which may act as a positive feedback by slowing the decay of adjacent ridges bounding the runnel (e.g. Fig. 10b). Where the background rate of cliff melt is low and winter refreeze persists on the cliff face, meltwater and debris conveyance may be the dominant ablative mechanism. This observed morphological heterogeneity is not considered in the top-edge delineation of an ice cliff, or in point-ablation stake measurements since placements are potentially spatially biased due to safety concerns (e.g. placement away from areas of falling or unstable debris). Therefore cliff parameterisation in dynamic glacier models still requires an improved processed-based understanding of cliff formation and evolution from field observations.

Isolating the magnitude of ice cliff retreat through multi-temporal observations is becoming possible with fine-resolution stereo imagery (e.g. Thompson et al. 2016) or low cost aerial surveys (e.g. Immerzeel et al. 2014; Brun et al. 2016). However, the steeply sloping cliff faces are likely to be poorly represented in commonly used 2D DEMs (Kolecka, 2012). Alternatively, fully 3D surveys could be pursued following a Structure-from-Motion with

Multi-view Stereo workflow (e.g. Smith et al. 2015) and 3D point cloud differencing (Lague et al., 2013) to reveal the spatial and temporal retreat dynamics across a range of cliff aspects. This technology facilitates comparisons at a spatial resolution comparable to that at which the processes are operating (Passalacqua et al., 2015) and cloud-to-cloud differencing is available in open source software (e.g. CloudCompare). These 3D measurements of cliff retreat could then be coupled to remote sensing observations of cliff spatio-temporal distribution for inclusion into dynamic glacier models, or used to validate cliff-scale grid-based models (e.g. Buri et al. 2016).

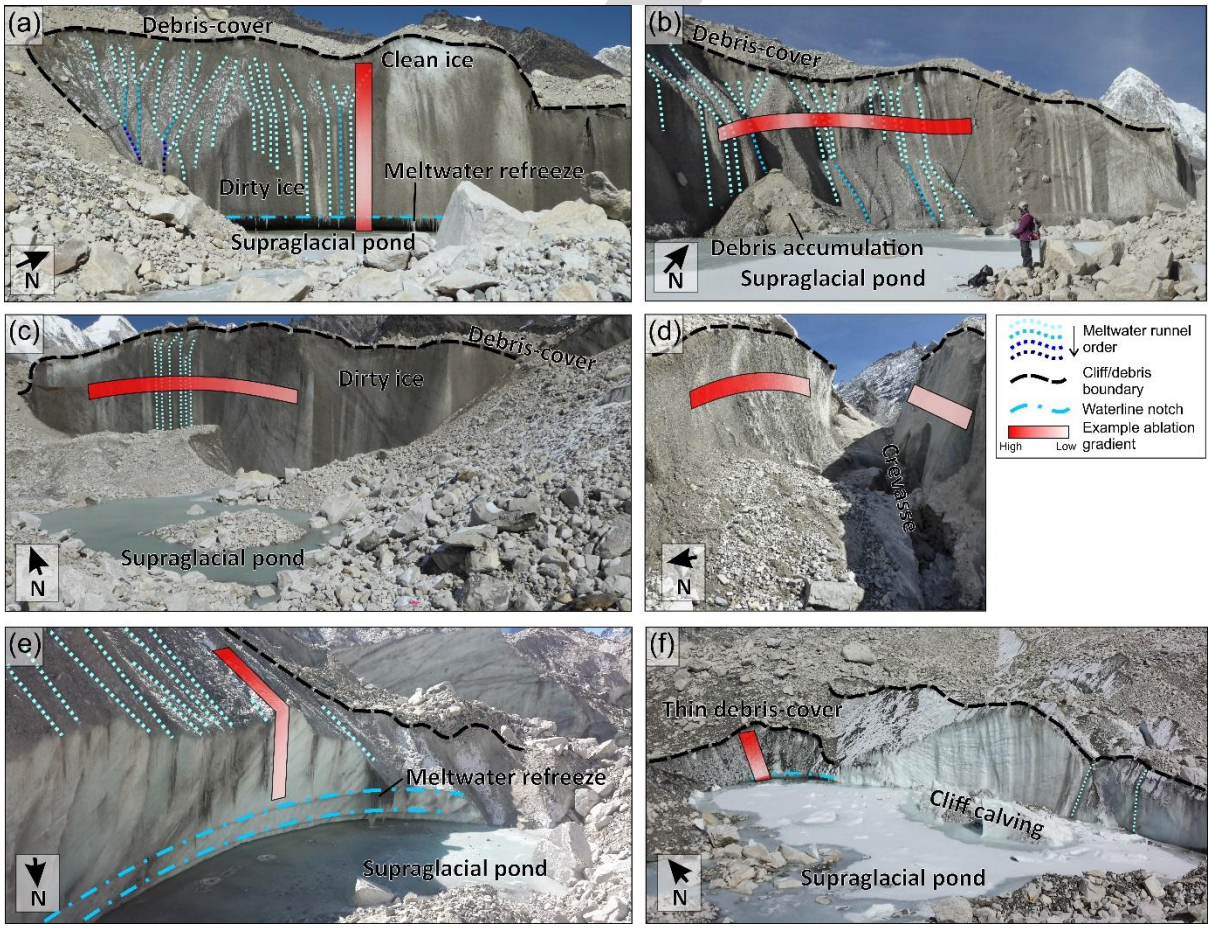

Figure 10. Examples of ice cliffs on the Khumbu Glacier. (a) An easterly facing cliff with well-developed meltwater channels, (b) a south-easterly facing cliff with well-developed meltwater runnels, (c) a south-facing cliff with limited meltwater runnels, (d) adjacent south- and north-facing cliffs with no meltwater runnels, (e) a cliff with historic water level notches revealing seasonal pond drainage, and (f) a south-facing debris-covered cliff and a west-facing clean-ice cliff with evidence of recent calving. Indicative ablation gradients are suggested from visual observations of cliff morphology and meltwater flows.

7. Conclusion and future work

We have presented the first spatio-temporally detailed analysis of ice cliff distribution and geometry characteristics for 14 debris-covered glaciers in the Everest region. Our results show that whilst ice cliffs are present across most of the debris-covered parts of these glaciers, their density is spatio-temporally variable and not clearly linked to glacier surface velocity. Therefore, ice cliffs do not appear to form preferentially on stagnating tongues where supraglacial ponds coalesce. However, we observed high spatial coincidence of ice cliffs and supraglacial ponds, highlighting the importance of the cliff-pond interaction and the potential transition from subaerial to calving ice cliff retreat, which is a transition that can increase cliff recession rates threefold (Benn et al., 2001). Supraglacial pond expansion in the region suggests this interaction may becoming increasingly pertinent (Watson et al., 2016).

The predominance of north-facing cliffs irrespective of glacier flow direction supports a strong solar radiation control on cliff evolution (e.g. Sakai et al. 2002). Here, a high direct solar radiation receipt on south-facing cliffs can promote rapid decay and burial under debris, whilst shaded north-facing cliffs can persist. However, increased temporal resolution is required to confirm the timescale over which this south-facing cliff decay occurs, compared to the temporal longevity of north-facing cliffs. Determining the interaction between cliff density, surface lowering, debris thickness, cliff aspect, energy balance fluxes, and the influence of supraglacial ponds, would all benefit from fully 3D multi-temporal observations of cliff evolution. By coupling remote sensing and in-situ observations it is possible to capture processes operating at multiple spatial scales on the heterogeneous cliff faces, which is necessary if the proper parameterisation of ice cliffs in dynamic glacier models is to be addressed.

To summarise, our main findings are:

(1) A high spatial coincidence of supraglacial ponds and ice cliffs where on average across the study glaciers 77 % of supraglacial pond area had an adjacent ice cliff, and 49 % of ice cliffs had an adjacent supraglacial pond.

(2) An increase in ice cliff density with distance up-glacier from the terminus to peak in the zone of active flow, before a decline towards the transition zone from debris to clean-ice.

(3) A spatial density of ice cliffs that is glacier-specific, and that is positively correlated with surface lowering and decreasing debris thickness up-glacier.

(4) A predominance of north-facing ice cliffs irrespective of glacier flow direction.

8. Acknowledgements

C.S.W acknowledges support from the School of Geography at the University of Leeds, the Mount Everest Foundation, the Royal Geographical Society (with IBG), the British Society for Geomorphology, the Petzl Foundation, and water@leeds. TerraSAR-X images were supplied by the European Space Agency under Category-1 Proposal Id. 32600 and we thank Adrian Luckman for use of his feature tracking code. Dhananjay Regmi and Himalayan Research Expeditions are thanked for invaluable support during fieldwork and for obtaining research permits. Owen King and David Rounce provided access to surface elevation change and debris-thickness datasets respectively. We thank three reviewers for comments, which helped improved this study.

References

Benn, D.I. Bolch, T. Hands, K. Gulley, J. Luckman, A. Nicholson, L.I. Quincey, D. Thompson, S. Toumi, R. and Wiseman, S. 2012. Response of debris-covered glaciers in the Mount Everest region to recent warming, and implications for outburst flood hazards. *Earth-Science Reviews.* **114**(1–2), 156-174.

Benn, D.I. Warren, C.R. and Mottram, R.H. 2007. Calving processes and the dynamics of calving glaciers. *Earth-Science Reviews.* **82**(3-4), 143-179.

Benn, D.I. Wiseman, S. and Hands, K.A. 2001. Growth and drainage of supraglacial lakes on debris-mantled Ngozumpa Glacier, Khumbu Himal, Nepal. *Journal of Glaciology.* **47**(159), 626-638.

Bolch, T. Buchroithner, M. Pieczonka, T. and Kunert, A. 2008. Planimetric and volumetric glacier changes in the Khumbu Himal, Nepal, since 1962 using Corona, Landsat TM and ASTER data. *Journal of Glaciology.* **54**(187), 592-600.

Bolch, T. Kulkarni, A. Kääb, A. Huggel, C. Paul, F. Cogley, J.G. Frey, H. Kargel, J.S. Fujita, K. Scheel, M. Bajracharya, S. and Stoffel, M. 2012. The State and Fate of Himalayan Glaciers. *Science.* **336**(6079), 310-314.

Bolch, T. Pieczonka, T. and Benn, D.I. 2011. Multi-decadal mass loss of glaciers in the Everest area (Nepal Himalaya) derived from stereo imagery. *The Cryosphere.* **5**(2), 349-358.

Brun, F. Buri, P. Miles, E.S. Wagnon, P. Steiner, J.F. Berthier, E. Ragettli, S. Kraaijenbrink, P. Immerzeel, W.W. and Pellicciotti, F. 2016. Quantifying volume loss from ice cliffs on debris-covered glaciers using high-resolution terrestrial and aerial photogrammetry. *Journal of Glaciology.* **FirstView**, 1-12.

Buri, P. Pellicciotti, F. Steiner, J.F. Miles, E.S. and Immerzeel, W.W. 2016. A grid-based model of backwasting of supraglacial ice cliffs on debris-covered glaciers. *Annals of Glaciology* **57**(71), 199-211.

Carrivick, J.L. and Tweed, F.S. 2013. Proglacial lakes: character, behaviour and geological importance. *Quaternary Science Reviews.* **78**, 34-52.

Chaturvedi, R.K. Kulkarni, A. Karyakarte, Y. Joshi, J. and Bala, G. 2014. Glacial mass balance changes in the Karakoram and Himalaya based on CMIP5 multi-model climate projections. *Climatic Change.* **123**(2), 315-328.

Douglas, J.S. Huss, M. Swift, D.A. Jones, J.M. and Salerno, F. 2016. Incorporating Distributed Debris Thickness in a Glacio-Hydrological Model: Khumbu Himalaya, Nepal. *The Cryosphere Discuss.* **2016**, 1-35.

Foster, L.A. Brock, B.W. Cutler, M.E.J. and Diotri, F. 2012. A physically based method for estimating supraglacial debris thickness from thermal band remote-sensing data. *Journal of Glaciology.* **58**(210), 677-691.

Gardelle, J. Arnaud, Y. and Berthier, E. 2011. Contrasted evolution of glacial lakes along the Hindu Kush Himalaya mountain range between 1990 and 2009. *Global and Planetary Change.* **75**(1–2), 47-55.

Gulley, J. and Benn, D.I. 2007. Structural control of englacial drainage systems in Himalayan debris-covered glaciers. *Journal of Glaciology.* **53**(182), 399-412.

Hambrey, M.J. 1977. Supraglacial drainage and its relationship to structure, with particular reference to Charles Rabots Bre, Okstindan, Norway. *Norsk Geografisk Tidsskrift - Norwegian Journal of Geography.* **31**(2), 69-77.

Han, H. Wang, J. Wei, J. and Liu, S. 2010. Backwasting rate on debris-covered Koxkar glacier, Tuomuer mountain, China. *Journal of Glaciology.* **56**(196), 287-296.

Haritashya, U.K. Pleasants, M.S. and Copland, L. 2015. Assessment of the evolution in velocity of two debris-covered glaciers in Nepal and New Zealand. *Geografiska Annaler: Series A, Physical Geography.* **97**(4), 737–751.

Immerzeel, W.W. Kraaijenbrink, P.D.A. Shea, J.M. Shrestha, A.B. Pellicciotti, F. Bierkens, M.F.P. and de Jong, S.M. 2014. High-resolution monitoring of Himalayan glacier dynamics using unmanned aerial vehicles. *Remote Sensing of Environment.* **150**, 93-103.

Inoue, J. 1977. Mass Budget of Khumbu Glacier. *Journal of the Japanese Society of Snow and Ice.* **39**(Special), 15-19.

Inoue, J. and Yoshida, M. 1980. Ablation and heat exchange over the khumbu glacier. *Journal of the Japanese Society of Snow and Ice.* **39**, 7-14.

Iwata, S., Watanabe, O. and Fushimi, H. 1980. Surface Morphology in the Ablation Area of the Khumbu Glacier. *Seppyo, 41 (Special issue).* **9-17**.

Juen, M. Mayer, C. Lambrecht, A. Han, H. and Liu, S. 2014. Impact of varying debris cover thickness on ablation: a case study for Koxkar Glacier in the Tien Shan. *The Cryosphere.* **8**(2), 377-386.

Kääb, A. Berthier, E. Nuth, C. Gardelle, J. and Arnaud, Y. 2012. Contrasting patterns of early twenty-first-century glacier mass change in the Himalayas. *Nature.* **488**(7412), 495-498.

Kääb, A. Treichler, D. Nuth, C. and Berthier, E. 2015. Brief Communication: Contending estimates of 2003-2008 glacier mass balance over the Pamir–Karakoram–Himalaya. *The Cryosphere.* **9**(2), 557-564.

King, O. Quincey, D.J. Carrivick, J.L. and Rowan, A.V. 2016. Spatial variability in mass change of glaciers in the Everest region, central Himalaya, between 2000 and 2015. *The Cryosphere Discuss.* **2016**, 1-35.

Kirkbride, M.P. 1993. The temporal significance of transitions from melting to calving termini at glaciers in the central Southern Alps of New Zealand. *The Holocene.* **3**(3), 232-240.

Kolecka, N. 2012. Vector algebra for Steep Slope Model analysis. *Landform Analysis.* **21**, 17-25.

Lague, D. Brodu, N. and Leroux, J. 2013. Accurate 3D comparison of complex topography with terrestrial laser scanner: Application to the Rangitikei canyon (N-Z). *ISPRS Journal of Photogrammetry and Remote Sensing.* **82**, 10-26.

Lutz, A.F. Immerzeel, W.W. Shrestha, A.B. and Bierkens, M.F.P. 2014. Consistent increase in High Asia's runoff due to increasing glacier melt and precipitation. *Nature Clim. Change.* **4**(7), 587-592.

Mattson, L.E. Gardner, J.S. and Young, G.J. 1993. Ablation of debris covered glaciers: An example from the Rakhiot Glacier, Punjab Himalaya. In: Young, G.J., ed. *Snow and Glacier Hydrology (Proceedings of the Kathmandu Symposium, November 1992)*, *Kathmandu, Nepal*. IAHS Publishing, 289-296.

Miles, E.S. Pellicciotti, F. Willis, I.C. Steiner, J.F. Buri, P. and Arnold, N.S. 2016. Refined energy-balance modelling of a supraglacial pond, Langtang Khola, Nepal. *Annals of Glaciology.* **57**(71), 29-40.

Nakawo, M. Iwata, S. Watanabe, O. and Yoshida, M. 1986. Processes which distribute supraglacial debris on the Khumbu Glacier, Nepal Himalaya. *Annals of Glaciology.* **8**, 129-131.

Nakawo, M. Yabuki, H. and Sakai, A. 1999. Characteristics of Khumbu Glacier, Nepal Himalaya: recent change in the debris-covered area. *Annals of Glaciology.* **28**(1), 118-122.

Nicholson, L. and Benn, D.I. 2006. Calculating ice melt beneath a debris layer using meteorological data. *Journal of Glaciology.* **52**(178), 463-470.

Nicholson, L. and Benn, D.I. 2013. Properties of natural supraglacial debris in relation to modelling sub-debris ice ablation. *Earth Surface Processes and Landforms.* **38**(5), 490-501.

Nie, Y. Zhang, Y. Ding, M. Liu, L. and Wang, Z. 2013. Lake change and its implication in the vicinity of Mt. Qomolangma (Everest), central high Himalayas, 1970–2009. *Environmental Earth Sciences.* **68**(1), 251-265.

Nuimura, T. Fujita, K. Yamaguchi, S. and Sharma, R.R. 2012. Elevation changes of glaciers revealed by multitemporal digital elevation models calibrated by GPS survey in the Khumbu region, Nepal Himalaya, 1992-2008. *Journal of Glaciology.* **58**(210), 648-656.

Östrem, G. 1959. Ice Melting under a Thin Layer of Moraine, and the Existence of Ice Cores in Moraine Ridges. *Geografiska Annaler.* **41**(4), 228-230.

Passalacqua, P. Belmont, P. Staley, D.M. Simley, J.D. Arrowsmith, J.R. Bode, C.A. Crosby, C. DeLong, S.B. Glenn, N.F. Kelly, S.A. Lague, D. Sangireddy, H. Schaffrath, K. Tarboton, D.G. Wasklewicz, T. and Wheaton, J.M. 2015. Analyzing high resolution topography for advancing the understanding of mass and energy transfer through landscapes: A review. *Earth-Science Reviews.* **148**, 174-193.

Pellicciotti, F. Stephan, C. Miles, E. Herreid, S. Immerzeel, W.W. and Bolch, T. 2015. Mass-balance changes of the debris-covered glaciers in the Langtang Himal, Nepal, from 1974 to 1999. *Journal of Glaciology.* **61**(226), 373-386.

Pfeffer, W.T. Arendt, A.A. Bliss, A. Bolch, T. Cogley, J.G. Gardner, A.S. Hagen, J.O. Hock, R. Kaser, G. Kienholz, C. Miles, E.S. Moholdt, G. Molg, N. Paul, F. Radic, V. Rastner, P. Raup, B.H. Rich, J.

Sharp, M.J. and Randolph, C. 2014. The Randolph Glacier Inventory: a globally complete inventory of glaciers. *Journal of Glaciology.* **60**(221), 537-552.

Quincey, D.J. Luckman, A. and Benn, D. 2009. Quantification of Everest region glacier velocities between 1992 and 2002, using satellite radar interferometry and feature tracking. *Journal of Glaciology.* **55**(192), 596-606.

Quincey, D.J. Richardson, S.D. Luckman, A. Lucas, R.M. Reynolds, J.M. Hambrey, M.J. and Glasser, N.F. 2007. Early recognition of glacial lake hazards in the Himalaya using remote sensing datasets. *Global and Planetary Change.* **56**(1–2), 137-152.

Racoviteanu, A.E. Arnaud, Y. Williams, M.W. and Manley, W.F. 2015. Spatial patterns in glacier characteristics and area changes from 1962 to 2006 in the Kanchenjunga–Sikkim area, eastern Himalaya. *The Cryosphere.* **9**(2), 505-523.

Reid, T.D. and Brock, B.W. 2014. Assessing ice-cliff backwasting and its contribution to total ablation of debris-covered Miage glacier, Mont Blanc massif, Italy. *Journal of Glaciology.* **60**(219), 3-13.

Reynolds, J.M. 2000. On the formation of supraglacial lakes on debris-covered glaciers. In: Nakawo, M.Raymond, C.F. and Fountain, A., eds. *IAHS Publ. 264 (Symposium at Seattle 2000 – Debris-Covered Glaciers)*, *Seattle, Washington, U.S.A*. IAHS Publishing, 153-161.

Rohl, K. 2006. Thermo-erosional notch development at fresh-water-calving Tasman Glacier, New Zealand. *Journal of Glaciology.* **52**(177), 203-213.

Rounce, D.R. and McKinney, D.C. 2014. Debris thickness of glaciers in the Everest area (Nepal Himalaya) derived from satellite imagery using a nonlinear energy balance model. *The Cryosphere.* **8**(4), 1317-1329.

Rowan, A.V. Egholm, D.L. Quincey, D.J. and Glasser, N.F. 2015. Modelling the feedbacks between mass balance, ice flow and debris transport to predict the response to climate change of debris-covered glaciers in the Himalaya. *Earth and Planetary Science Letters.* **430**, 427-438.

Sakai, A. Nakawo, M. and Fujita, K. 1998. Melt rate of ice cliffs on the Lirung Glacier, Nepal Himalayas. *Bulletin of Glaciological Research.* **16**, 57-66.

Sakai, A. Nakawo, M. and Fujita, K. 2002. Distribution characteristics and energy balance of ice cliffs on debris-covered glaciers, Nepal Himalaya. *Arctic Antarctic and Alpine Research.* **34**(1), 12-19.

Sakai, A. Nishimura, K. Kadota, T. and Takeuchi, N. 2009. Onset of calving at supraglacial lakes on debris-covered glaciers of the Nepal Himalaya. *Journal of Glaciology.* **55**(193), 909-917.

Sakai, A. Takeuchi, N. Fujita, K. and Nakawo, M. 2000. Role of supraglacial ponds in the ablation process of a debris-covered glacier in the Nepal Himalayas. In: Nakawo, M.Raymond, C.F. and Fountain, A., eds. *IAHS Publ. 264 (Symposium at Seattle 2000 – Debris-Covered Glaciers)*, *Seattle, Washington, U.S.A*. IAHS Publishing, 119-130.

Salerno, F. Guyennon, N. Thakuri, S. Viviano, G. Romano, E. Vuillermoz, E. Cristofanelli, P. Stocchi, P. Agrillo, G. Ma, Y. and Tartari, G. 2015. Weak precipitation, warm winters and springs impact glaciers of south slopes of Mt. Everest (central Himalaya) in the last 2 decades (1994–2013). *The Cryosphere.* **9**(3), 1229-1247.

Salerno, F. Thakuri, S. D'Agata, C. Smiraglia, C. Manfredi, E.C. Viviano, G. and Tartari, G. 2012. Glacial lake distribution in the Mount Everest region: Uncertainty of measurement and conditions of formation. *Global and Planetary Change.* **92-93**, 30-39.

Scherler, D. Bookhagen, B. and Strecker, M.R. 2011. Spatially variable response of Himalayan glaciers to climate change affected by debris cover. *Nature Geosci.* **4**(3), 156-159.

Shea, J.M. and Immerzeel, W.W. 2016. An assessment of basin-scale glaciological and hydrological sensitivities in the Hindu Kush–Himalaya. *Annals of Glaciology.* **57**(71), 308-318.

Shea, J.M. Immerzeel, W.W. Wagnon, P. Vincent, C. and Bajracharya, S. 2015. Modelling glacier change in the Everest region, Nepal Himalaya. *The Cryosphere.* **9**(3), 1105-1128.

Shrestha, A.B. and Aryal, R. 2011. Climate change in Nepal and its impact on Himalayan glaciers. *Regional Environmental Change.* **11**, 65-77.

Smith, M.W. Carrivick, J.L. and Quincey, D.J. 2015. Structure from motion photogrammetry in physical geography. *Progress in Physical Geography.*

Soncini, A. Bocchiola, D. Confortola, G. Minora, U. Vuillermoz, E. Salerno, F. Viviano, G. Shrestha, D. Senese, A. Smiraglia, C. and Diolaiuti, G. 2016. Future hydrological regimes and glacier cover in the Everest region: The case study of the upper Dudh Koshi basin. *Science of The Total Environment.* **565**, 1084-1101.

Steiner, J.F. and Pellicciotti, F. 2016. Variability of air temperature over a debris-covered glacier in the Nepalese Himalaya. *Annals of Glaciology.* **57**(71), 295-307.

Steiner, J.F. Pellicciotti, F. Buri, P. Miles, E.S. Immerzeel, W.W. and Reid, T.D. 2015. Modelling ice-cliff backwasting on a debris-covered glacier in the Nepalese Himalaya. *Journal of Glaciology.* **61**(229), 889-907.

Thakuri, S. Salerno, F. Bolch, T. Guyennon, N. and Tartari, G. 2016. Factors controlling the accelerated expansion of Imja Lake, Mount Everest region, Nepal. *Annals of Glaciology.* **57**(71), 245-257.

Thakuri, S. Salerno, F. Smiraglia, C. Bolch, T. D'Agata, C. Viviano, G. and Tartari, G. 2014. Tracing glacier changes since the 1960s on the south slope of Mt. Everest (central Southern Himalaya) using optical satellite imagery. *Cryosphere.* **8**(4), 1297-1315.

Thompson, S. Benn, D. Mertes, J. and Luckman, A. 2016. Stagnation and mass loss on a Himalayan debris-covered glacier: processes, patterns and rates. *Journal of Glaciology.* **FirstView**, 1-19.

Thompson, S.S. Benn, D.I. Dennis, K. and Luckman, A. 2012. A rapidly growing moraine-dammed glacial lake on Ngozumpa Glacier, Nepal. *Geomorphology.* **145**, 1-11.

Wang, W.C. Xiang, Y. Gao, Y. Lu, A.X. and Yao, T.D. 2015. Rapid expansion of glacial lakes caused by climate and glacier retreat in the Central Himalayas. *Hydrological Processes.* **29**(6), 859-874.

Watson, C.S. Quincey, D.J. Carrivick, J.L. and Smith, M.W. 2016. The dynamics of supraglacial ponds in the Everest region, central Himalaya. *Global and Planetary Change.* **142**, 14-27.

Yang, X. Zhang, T. Qin, D. Kang, S. and Qin, X. 2011. Characteristics and Changes in Air Temperature and Glacier's Response on the North Slope of Mt. Qomolangma (Mt. Everest). *Arctic, Antarctic, and Alpine Research.* **43**(1), 147-160.

Yang, X. Zhang, Y. Zhang, W. Yan, Y. Wang, Z. Ding, M. and Chu, D. 2006. Climate change in Mt. Qomolangma region since 1971. *Journal of Geographical Sciences.* **16**(3), 326-336.

Ye, Q. Bolch, T. Naruse, R. Wang, Y. Zong, J. Wang, Z. Zhao, R. Yang, D. and Kang, S. 2015. Glacier mass changes in Rongbuk catchment on Mt. Qomolangma from 1974 to 2006 based on topographic maps and ALOS PRISM data. *Journal of Hydrology.* **530**, 273-280.

Zhang, Y. Fujita, K. Liu, S. Liu, Q. and Nuimura, T. 2011. Distribution of debris thickness and its effect on ice melt at Hailuogou glacier, southeastern Tibetan Plateau, using in situ surveys and ASTER imagery. *Journal of Glaciology.* **57**(206), 1147-1157.

Zhao, L. Ding, R. and Moore, J.C. 2014. Glacier volume and area change by 2050 in high mountain Asia. *Global and Planetary Change.* **122**, 197-207.

Supplementary information

Date	Description	Ama Dablam	Barun	Changri Nup	Changri Shar	Gaunara	Imja	Kangshung	Khumbu	Lhotse	Lhotse Nup	Lhotse Shar	Ngozumpa	Nuptse	Rongbuck
18/12/2000	No of cliffs	71													
	No of ponds	44*													
	Total cliff length (m)	5,060 ± 631													
	Total pond area (m^2)	25,128													
07/05/2003	No of cliffs									317	57			144	
	No of ponds									313	76			164	
	Total cliff length (m)									15,003 ± 1,300	2,222 ± 234			6,337 ± 590	
	Total pond area (m^2)									230,244	31,204			86,552	
24/05/2009	No of cliffs						168					459			
	No of ponds						71					260			
	Total cliff length (m)						8,422 ± 1,025					22,643 ± 2,800			
	Total pond area (m^2)						28,410					139,773			
03/11/2009	No of cliffs	75		121	125	249			436	299	59			164	582
	No of ponds	43*		101	80	162			191*	312	67			131	396
	Total cliff length (m)	6,126 ± 435		9,548 ±702	6,006 ±725	15,623 ± 1,444			23,364 ± 2,529	16,607 ± 1,734	2,698 ± 342			8,097 ± 951	40,015 ± 3,376
	Total pond area (m^2)	46,489		182,985	45,569	85,476			131,929	129,337	22,764			39,576	433,853
09/06/2010	No of cliffs												1,633		
	No of ponds												915*		
	Total cliff length (m)												72,183 ± 7,185		
	Total pond area (m^2)												742,807		
13/05/2015	No of cliffs	75	371				122	663		293	71	289		188	654
	No of ponds	63	231				58	679		335	100	200		149	567
	Total cliff length (m)	5,893 ± 398	20,008 ± 2,003				5998 ± 659	42,398 ± 3,580		17,226 ± 1,582	2,695 ± 383	15,956 ± 1,561		8,693 ± 1,015	39,711 ± 3,532
	Total pond area (m^2)	73,196	118,828				22,360	408,782		255,585	38,729	83,139		77,427	357,334
07/06/2015	No of cliffs			205	159	309			520						
	No of ponds			118	138	230			303						
	Total cliff length (m)			11,583 ±861	6,136 ± 668	17,407 ± 1,298			27,862 ± 2,184						
	Total pond area (m^2)			324755	57,174	203,502			306,571						

Data for images without complete glacier coverage are excluded
* Indicates supraglacial pond dataset from Watson et al. (2016)

Supplementary Table 1. Ice cliff and supraglacial pond characteristics

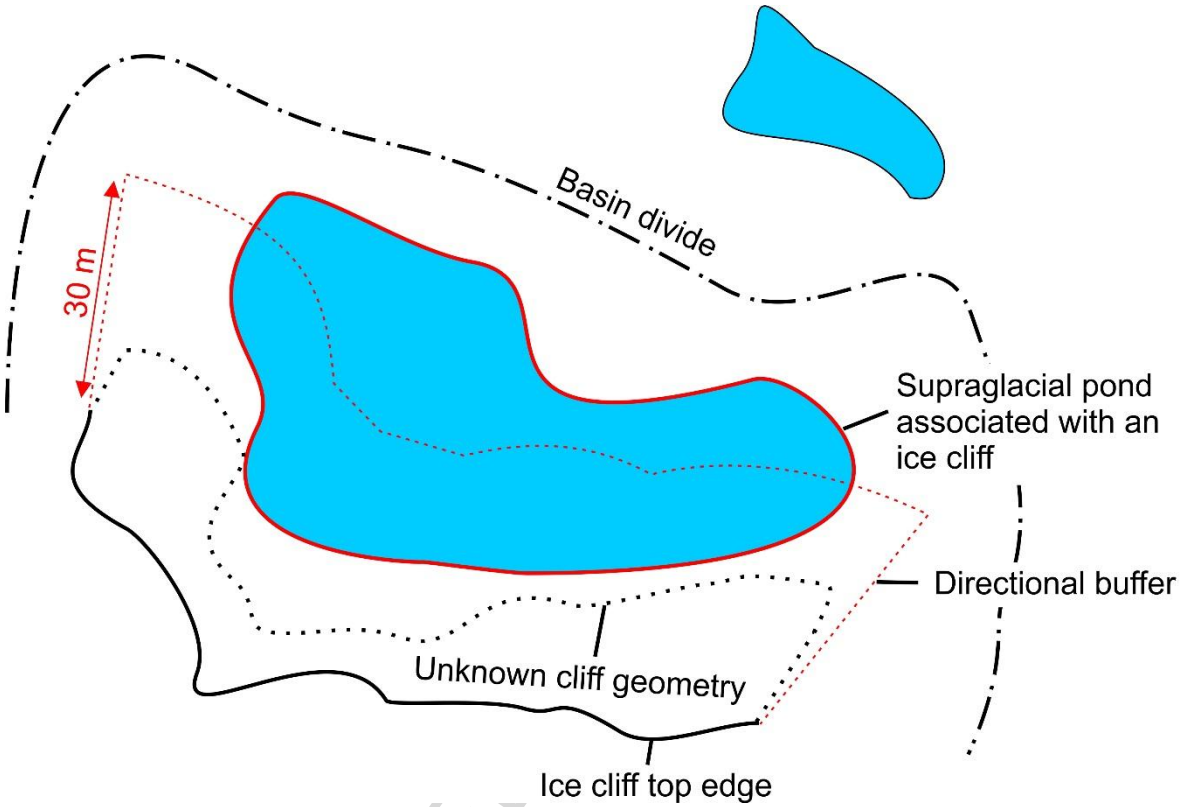

Supplementary Figure 1. A 30 m directional buffer is used to analyse supraglacial pond and ice cliff coincidence, accounting for an unknown cliff geometry.

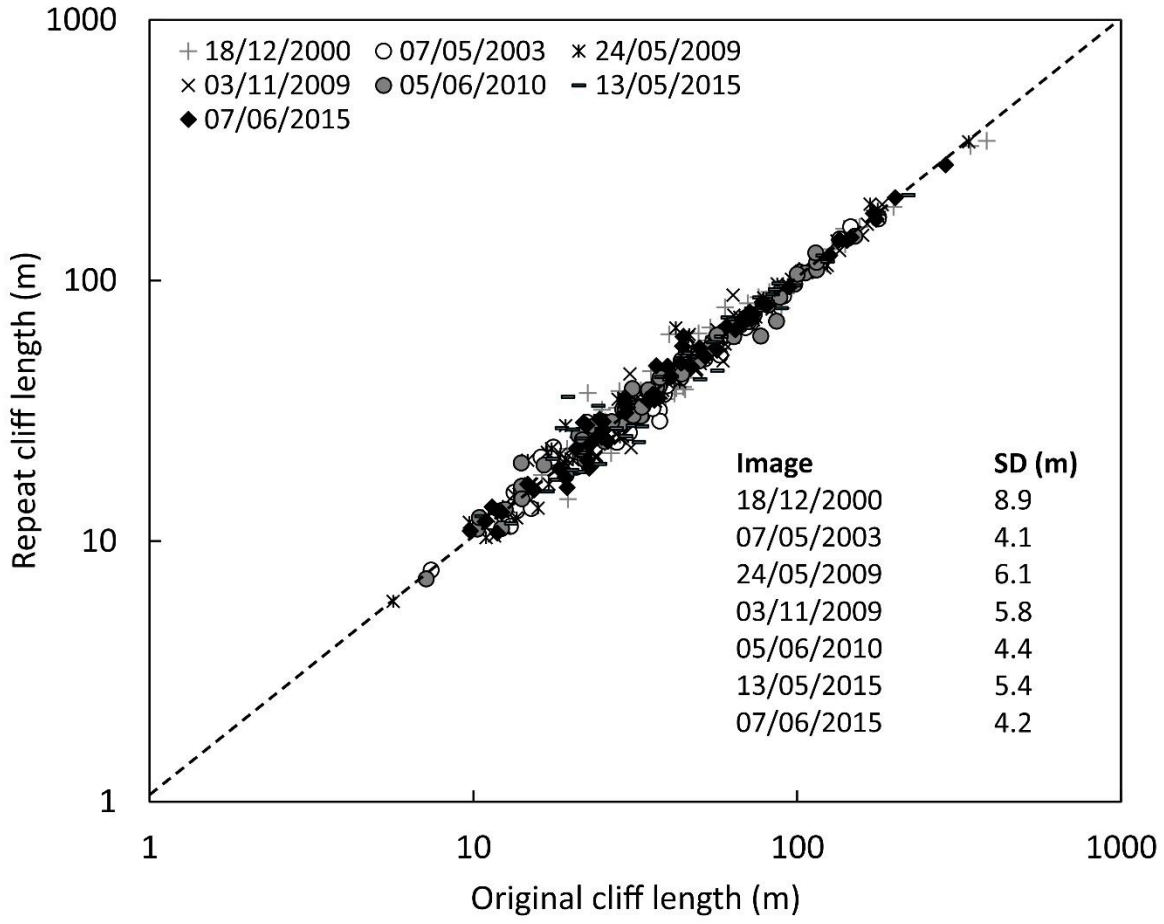

Supplementary Figure 2. Operator repeatability assessment from the repeat digitisation of 60 cliffs in each time period. Standard deviations are shown, which are used in Figure 4.

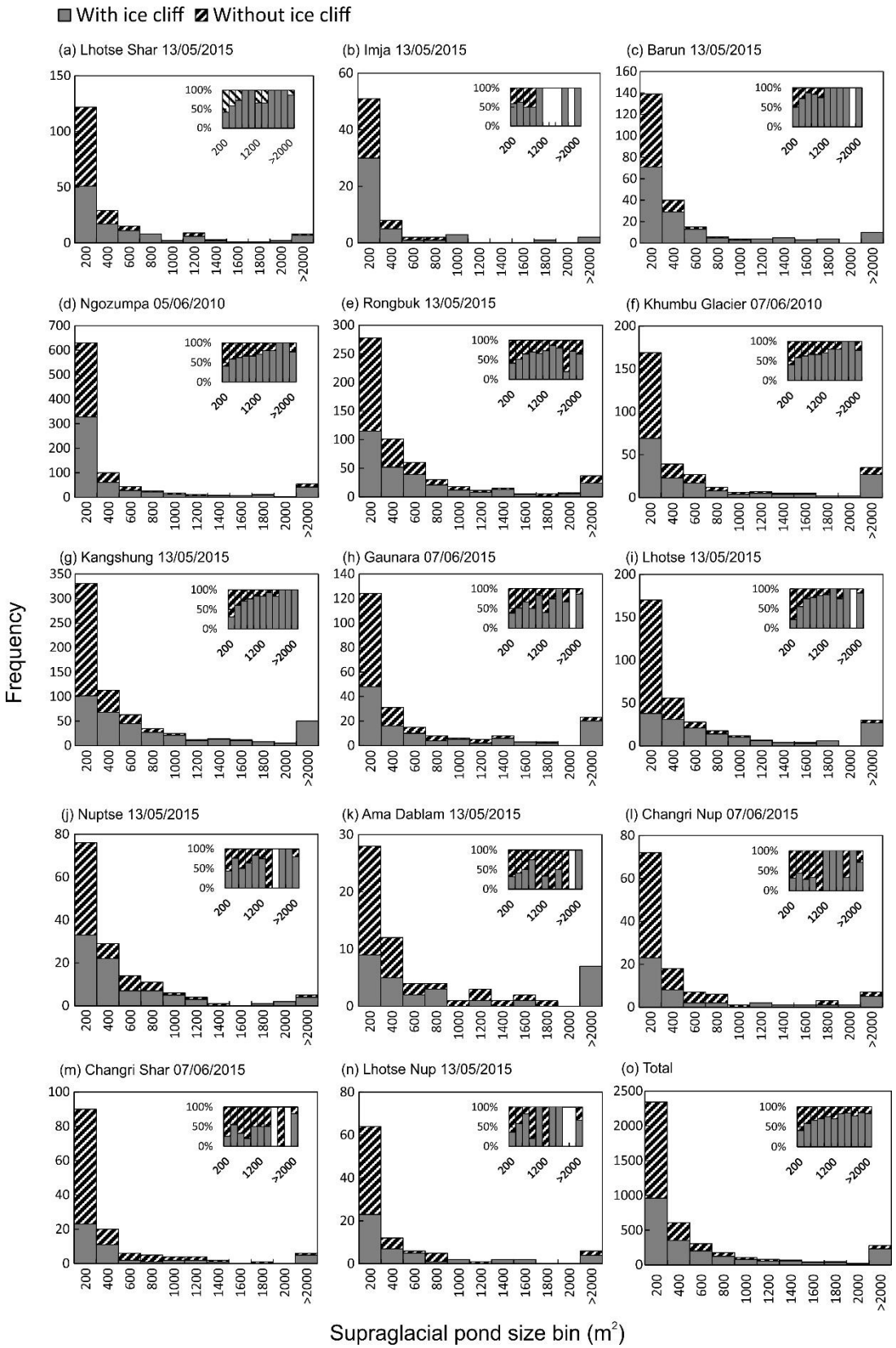

Supplementary Figure 3. The size distribution of supraglacial ponds and coincidence with ice cliffs, shown for the most recent time period for each glacier. Insets show the same data as a percentage distribution.

Highlights:

- We analysed ice cliffs and supraglacial ponds on 14 glaciers (2000 – 2015)
- Ice cliffs predominantly had north-facing aspects, independent of glacier flow direction
- Ice cliff density was positively correlated with surface lowering
- Ice cliff density peaked within zones of active ice flow
- 49 % of ice cliffs featured an adjacent supraglacial pond